Physica D 446 (2023) 133675

Contents lists available at ScienceDirect

Physica D

journal homepage: www.elsevier.com/locate/physd

A direct method approach for data-driven inference of high accuracy adaptive phase-isostable reduced order models

Dan Wilson

Department of Electrical Engineering and Computer Science, University of Tennessee, Knoxville, TN 37996, USA

ARTICLE INFO

Article history:
Received 10 October 2022
Received in revised form 16 December 2022
Accepted 28 January 2023
Available online 1 February 2023
Communicated by L. Huang

Keywords:
Phase reduction
Isostable coordinates
Data-driven
Model identification
Phase–amplitude reduction
Circadian rhythms

ABSTRACT

Phase–amplitude reduction techniques have shown great promise for identifying analytically tractable reduced order models in applications involving strongly perturbed and strongly coupled oscillatory dynamical systems. However, efficient methods for inference of these reduced order models from data are still needed. In this work, a data-driven strategy for inference of the necessary terms comprising an adaptive phase-isostable reduced order model is proposed. This strategy requires no more data than the well-established direct method used for obtaining standard phase reduced models, i.e., the application of a series of pulse inputs and the subsequent examination of the relaxation to the underlying limit cycle. Illustrative examples are provided for a collection of numerical models where the resulting adaptive phase-isostable reduced order equations are substantially more accurate than models obtained using standard phase reduction.

1. Introduction

Phase reduction is a well-established strategy for reducing the complexity and dimensionality of oscillatory dynamical systems [1–4]. Using this strategy, a system with a stable limit cycle of the general form

$$\dot{x} = F(x, u), \tag{1}$$

where F determines the system dynamics, $x \in \mathbb{R}^N$ denotes the system state, and $u \in \mathbb{R}^M$ corresponds to an input can be represented according to

$$\dot{\theta} = \omega + Z(\theta)u(t). \tag{2}$$

Above, $\theta \in [0, 2\pi)$ encodes for oscillation timing, ω is the unperturbed natural frequency that results when taking $u(t) = 0$, and $Z(\theta)$ is a row vector, often referred to as the infinitesimal phase response curve, that characterizes the phase shifts in response to small inputs. The phase reduction strategy considers oscillatory dynamics not in terms of the N-dimensional state, but rather, in terms of the (one dimensional) oscillation timing yielding a tremendous reduction in dimensionality. Indeed, this approach has been used successfully in many applications where the analysis would otherwise be intractable [4–8].

In situations where the underlying model equations are unknown, $Z(\theta)$ from Eq. (2) can be approximated from data using the direct method [2,9,10]. As a brief description, consider the application of a short pulse of input $u(t) = me_i$ at a known phase θ_0 lasting t_0 time units where $e_i \in \mathbb{R}^M$ is the ith component of the standard unit basis and $m \in \mathbb{R}$ sets the magnitude of the pulse input. By inferring the change in phase $\Delta\theta$ in response to this input, a pointwise estimate of the infinitesimal phase response curve can be estimated according to

$$Z(\theta_0)e_i \approx \frac{\Delta\theta}{mt_0}, \tag{3}$$

By repeating this procedure for multiple choices of θ_0 and for each dimension of the input, $Z(\theta)$ can be inferred by fitting a curve to the resulting data. As a concrete example, consider a conductance-based model neuron of the form (A.1) from Appendix A taking the baseline current $i_b = 8\ \mu\text{A/cm}^2$ with an additional transmembrane current input $u(t) \in \mathbb{R}$ added to the transmembrane voltage variable. Fig. 1 illustrates an application of the direct method for inputs of varying magnitudes. Panel A shows the response to the example pulse from Panel B which results in the phase shift $\Delta\theta$. Panel C shows the inferred phase response curve with measurements taken according to (3) for inputs of various magnitudes.

Fig. 1 illustrates the primary shortcoming of standard phase reduction — its limited accuracy beyond the weakly perturbed limit. In many practical applications, the applied inputs are far larger than the weakly perturbed limit rendering the phase reduction unusable. A variety of methods have been proposed to better characterize the phase dynamics when larger magnitude inputs are used. For instance, the notion of a residual phase response curve [11–13] has been suggested to characterize how

E-mail address: dwilso81@utk.edu.

https://doi.org/10.1016/j.physd.2023.133675
0167-2789/

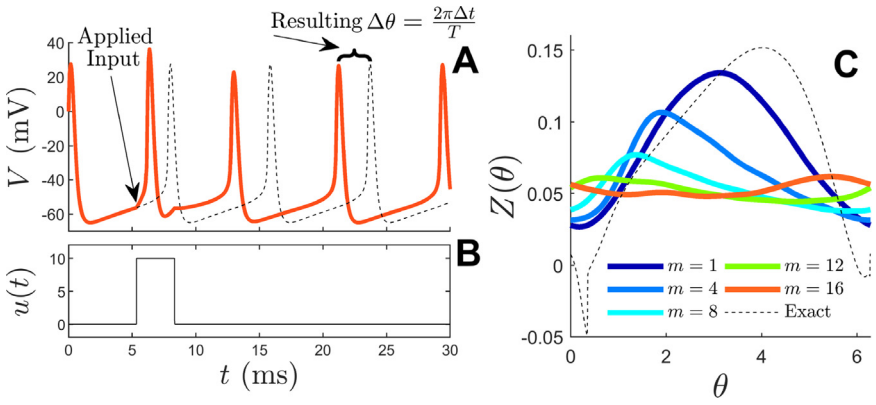

Fig. 1. The direct method is applied to infer the infinitesimal phase response curve from Eq. (2) for a conductance-based model neuron of the form (A.1) from Appendix A with an additional transmembrane current input $u(t) \in \mathbb{R}$ added to the transmembrane voltage variable. Panel A illustrates the response to the pulse input shown in panel B. The red line shows the perturbed response and the dashed line shows the voltage output that would have resulted if the pulse input had not been applied. Panel C shows the effective infinitesimal phase response curve inferred according to Eq. (3) using pulses of various magnitudes m (in $\mu A/cm^2$). For small magnitude inputs, the resulting $Z(\theta)$ is close to the infinitesimal phase response curve (i.e., $\partial\theta/\partial V$ which is shown as a dashed line). As the pulse magnitude becomes larger, the effective change in phase deviates unpredictably from the true infinitesimal phase response curve.

inputs influence the oscillation timing over multiple periods. Other methods have been developed to understand the phase response to arbitrarily large but slowly [14,15] or rapidly [16] varying inputs. Iterated mapping techniques have also been proposed to consider entrainment of strongly perturbed oscillators to periodic inputs [17,18].

Generally, the phase reduction (2) begins to break down when the magnitude of the applied input is large relative to the size of the smallest magnitude Floquet exponent (which sets the relaxation rate of perturbed solutions back to the limit cycle [19]). Large inputs can drive the state far from the underlying limit cycle so that the infinitesimal phase response curve, which depends on the gradient of the phase with respect to the state evaluated on the limit cycle, no longer provides an accurate approximation of the true response to input. In these situations, amplitude-based effects must be considered in conjunction with the phase dynamics. A variety of phase–amplitude coordinate systems have been suggested in recent years [14,20–25]. The amplitude coordinates can be used to characterize how the phase dynamics change as the state is perturbed from the limit cycle [26]. Additionally, asymptotic expansions of the phase dynamics in a basis of amplitude coordinates can be helpful for obtaining reduced order equations that are valid for large magnitude inputs [27,28] and for considering phase locking between strongly coupled oscillators [25,29,30]. Phase–amplitude reduction techniques have shown great promise for identifying analytically tractable, reduced order models that are valid in the strongly perturbed regime, however, implementation typically requires knowledge of the underlying dynamical equations. Data-driven methods for inference of phase–amplitude-based models are often numerically sensitive to measurement noise, especially when considering asymptotic expansions to high orders of accuracy, limiting implementation in many practical applications.

In this work, data-driven strategies for inference of the necessary terms comprising an adaptive phase–amplitude reduction are considered. Introduced in [31], the adaptive phase–amplitude reduction considers a collection of periodic orbits that results as a given parameter set changes. By actively updating the effective system parameters in order to keep the amplitude coordinates small, a resulting reduced order model can be obtained that is valid far beyond the weakly perturbed limit. In the implementation of this strategy, it is often useful to use isostable coordinates, which are formally defined as level sets of the slowest decaying eigenfunctions of the Koopman operator [32,33], to encode for amplitude-based effects.

Through direct analysis of the equations that underlie the adaptive phase-isostable reduction, this work illustrates that all necessary terms can be inferred by simply measuring a set of infinitesimal phase and isostable response curves (for instance using the direct method or other previously established data-driven strategies [23,34]). In other words, if infinitesimal phase and isostable response curves can be inferred accurately from data, the adaptive phase-isostable reduction can be readily implemented which is generally substantially more accurate than standard phase reduction (2). Furthermore, all necessary terms of the adaptive phase-isostable reduction can also be inferred solely from a series of step function inputs, as opposed to pulsatile inputs typically used for the direct method. By contrast, a previously proposed strategy from [35] required the application of *both* pulse and step function inputs to infer the necessary terms of the phase-isostable reduction. The analysis provided in this work illustrates that either step function inputs or pulse inputs can be used, and that they ultimately provide redundant information.

The organization of this paper is as follows: Section 2 provides necessary background on the phase, isostable, and adaptive phase-isostable coordinate systems used throughout this work. Section 3 gives a detailed analysis of the terms that comprise the adaptive phase-isostable coordinate reduction, ultimately showing that all necessary terms can be determined with knowledge of the infinitesimal phase response curve along with the infinitesimal isostable response curve and Floquet exponent associated with each isostable coordinate. These relationships suggest an efficient method for inference of the adaptive phase-isostable reduced order equations that require the same data as the well-established direct method. Section 4 provides illustrative examples for a collection of numerical models and Section 5 provides concluding remarks.

2. Background

2.1. Phase coordinates and phase reduction

Consider a general ordinary differential equation of the form (1). Suppose that for a constant choice of $u = u_0$, Eq. (1) has a stable T-periodic orbit $x^{\gamma}_{u_0}$. Isochrons [2,36], which represent sets of initial conditions that have the same asymptotic convergence to the limit cycle, can be used to define phase for all states in the basin of attraction of the limit cycle. More precisely, letting θ_1 be the phase corresponding to an arbitrary initial condition

$a(0) \in x^{\gamma}_{u_0}$, the θ_1 isochron, Γ_{θ_1} corresponds to the set of all $b(0)$ such that

$$\lim_{t\to\infty} \|a(t) - b(t)\| = 0, \tag{4}$$

where $\|\cdot\|$ can be any vector norm. Using isochrons defined according to Eq. (4) allows for the definition of a phase $\theta(x, u_0) \in [0, 2\pi)$ for all states $x \in x^{\gamma}_{u_0}$ scaled so that $d\theta/dt = 2\pi/T = \omega$ under the flow of (1) when taking $u = u_0$. Restricting one's attention to a close neighborhood of the limit cycle, changing variables yields the phase reduction that captures the phase dynamics for inputs that differ from u_0

$$\begin{aligned}\frac{d\theta}{dt} &= \frac{\partial\theta}{\partial x}\cdot\frac{dx}{dt}\\ &= \frac{\partial\theta}{\partial x}\cdot\left(F(x,u_0) + \frac{\partial F}{\partial u}(u-u_0) + O(\|u-u_0\|^2)\right)\\ &= \omega(u_0) + Z(\theta,u_0)(u-u_0) + O(\|u-u_0\|^2)\\ &\quad + O(\|x - x^{\gamma}_{u_0}(\theta)\|^2),\end{aligned} \tag{5}$$

where $Z(\theta, u_0) = \left(\frac{\partial\theta}{\partial x}\right)^T \frac{\partial F}{\partial u}$ with all partial derivatives evaluated at $x = x^{\gamma}_{u_0}(\theta)$ and $u = u_0$, the 'dot' denotes the dot product, and ^{T} indicates the vector transpose. In the final line of the equation above, $\frac{\partial\theta}{\partial x}\cdot F(x, u_0) = \omega(u_0)$ because $\dot\theta = \omega(u_0)$ when $u(t) = u_0$. Eq. (5) can be used to analyze the N-dimensional Eq. (1) in terms of a 1-dimensional phase. However, note that the truncation errors grow as both $u - u_0$ and the distance from the limit cycle increase. As such, Eq. (5) is only valid in the weakly perturbed limit [1,2,4], i.e., when $u - u_0 = O(\epsilon)$ where $0 < \epsilon \ll 1$. It can still be applied for systems with noninfinitesimal inputs, but it is not guaranteed to match the behavior of the underlying dynamical system (1) in this case. This point is highlighted in Fig. 1.

2.2. Isostable coordinates and phase-isostable reduction

In order to improve the accuracy of the standard phase reduction from Eq. (5), information about the amplitude dynamics must be considered. These amplitude dynamics generally refer to the transient behavior in directions transverse to the limit cycle. A variety of coordinate systems have been proposed [21–23,25,28] that consider the amplitude dynamics. The isostable coordinate framework, which encodes for level sets of the slowest decaying modes of the Koopman operator [32,37], will be considered in this work. When restricting one's attention to a close neighborhood of the limit cycle, isostable coordinates have a direct relationship with Floquet coordinates. Defining taking $u = u_0$ and defining $\Delta x = x - x^{\gamma}_{u_0}(\theta)$, to a linear approximation

$$\Delta\dot{x} = J\Delta x, \tag{6}$$

where J is the Jacobian evaluated at $x^{\gamma}_{u_0}(\theta(t))$. Let Φ denote the monodromy matrix, i.e., with the relationship $\Delta x(T) = \Phi\Delta x(0)$. If Φ is diagonalizable, near $x^{\gamma}_{u_0}$ solutions of (1) follow [28]

$$x - x^{\gamma}_{u_0}(\theta) = \sum_{j=1}^{N-1} \psi_j g^j(\theta, u_0) + O(\psi_1^2) + \cdots + O(\psi_{N-1}^2). \tag{7}$$

Above, each $g^j(\theta, u_0)$ is a Floquet eigenfunction associated with the time varying linear Eq. (6), and $\psi_1, \ldots, \psi_{N-1}$ are isostable coordinates associated with the periodic orbit $x^{\gamma}_{u_0}$. For linear time-varying systems, isostable coordinates are often referred to as Floquet coordinates. In contrast to Floquet coordinates, however, isostable coordinates can be defined in the entire basin of attraction of the limit cycle as level sets of the most slowly decaying eigenfunctions of the Koopman operator [32,38]; when taking $u = u_0$ to be constant, these isostable coordinates have dynamics $\dot\psi_j = \kappa_j(u_0)\psi_j$ so that they decay exponentially. Above, $\kappa_j(u_0)$ is the Floquet exponent associated with the jth isostable coordinate for the periodic orbit $x^{\gamma}_{u_0}$. Similar to Eq. (5), through a change of variables one can consider the dynamics of any isostable coordinate for inputs that differ from u_0:

$$\begin{aligned}\frac{d\psi_j}{dt} &= \frac{\partial\psi_j}{\partial x}\cdot\frac{dx}{dt}\\ &= \frac{\partial\psi_j}{\partial x}\cdot\left(F(x,u_0) + \frac{\partial F}{\partial u}(u-u_0) + O(\|u-u_0\|^2)\right)\\ &= \kappa_j(u_0)\psi_j + I_j(\theta,u_0)(u-u_0) + O(\|u-u_0\|^2)\\ &\quad + O(\|x - x^{\gamma}_{u_0}(\theta)\|^2),\end{aligned} \tag{8}$$

for $j = 1, \ldots, N-1$ where $I_j(\theta, u_0) = \left(\frac{\partial\psi_j}{\partial x}\right)^T \frac{\partial F}{\partial u}$ with all partial derivatives evaluated at $x = x^{\gamma}_{u_0}(\theta)$ and $u = u_0$. In the final line above, $\frac{\partial\psi_j}{\partial x}\cdot F(x, u_0) = \kappa_j(u_0)\psi_j$ because $\dot\psi_j = \kappa_j(u_0)\psi_j$ when $u(t) = u_0$. Truncating the higher order terms from Eq. (8), the phase reduction from (5) can be augmented with isostable coordinates:

$$\begin{aligned}&\dot\theta = \omega(u_0) + Z(\theta,u_0)(u-u_0),\\ &\dot\psi_j = \kappa_j(u_0)\psi_j + I_j(\theta,u_0)(u-u_0),\\ &\quad j = 1,\ldots,N-1.\end{aligned} \tag{9}$$

In many cases, a subset of the Floquet exponents will have large magnitude real components so that the associated isostable coordinates decay rapidly. Ignoring these rapidly decaying isostable coordinates (assuming they are zero), $\beta < N-1$ isostable coordinates can be considered in (9) yielding a reduced order set of equations. Note that while Eq. (9) does take amplitude dynamics into account, it is still only valid in the weakly perturbed limit and generally breaks down when using large magnitude inputs. The adaptive phase-isostable reduction strategy described in the following section can be used to overcome this limitation by considering the dynamics in reference to a continuous family of limit cycles.

2.3. Adaptive phase-isostable reduction

Following the adaptive phase-isostable reduction formulation considered in [31,35], one can consider an additional set of variables $p \in \mathbb{R}^M$ in the same space as the inputs with dynamics that will be described momentarily. It will be assumed that when p is held constant, for some set of allowable p, the differential equation $\dot x = F(x, p)$ has a stable periodic orbit x^{γ}_p. For each x^{γ}_p, a corresponding phase $\theta(x, p)$ and set of isostable coordinates $\psi_1(x, p), \ldots, \psi_\beta(x, p)$ can be defined. As discussed in [31], the phase coordinates associated with each $x^{\gamma}_p(\theta)$ are unique up to a constant shift. These shifts can be explicitly defined, for instance, using a Poincaré section to correspond to a level set of the phases between limit cycles.

To proceed, one can rewrite Eq. (1) as

$$\dot x = F(x,p) + U_e(x,u,p), \tag{10}$$

where

$$\begin{aligned}U_e(x,u,p) &= F(x,u) - F(x,p)\\ &= \frac{\partial F}{\partial u}(u-p) + O(\|u-p\|^2),\end{aligned} \tag{11}$$

where all partial derivatives are evaluated at x taking $u = p$. In Eq. (10), $F(x, p)$ represents the nominal behavior of the system (1) when taking $u = p$. The term $U_e(x, u, p)$ can be thought of as an effective input. Using this formulation, let p be nonstatic. Changing variables to work in a basis of phase and isostable coordinates yields

$$\frac{d}{dt}\theta(x,p) = \frac{\partial\theta}{\partial x}\cdot\frac{dx}{dt} + \frac{\partial\theta}{\partial p}\cdot\frac{dp}{dt},$$

$$\frac{d}{dt}\psi_j(x,p) = \frac{\partial \psi_j}{\partial x}\cdot\frac{dx}{dt} + \frac{\partial \psi_j}{\partial p}\cdot\frac{dp}{dt},$$
$$j = 1,\dots,\beta,$$
$$\frac{dp}{dt} = G_p(p,\theta,\psi_1,\dots,\psi_\beta), \tag{12}$$

where G_p determines how p changes in time which will be considered more carefully momentarily. Eq. (12) can be simplified by noting that $\frac{\partial\theta}{\partial x}\cdot\frac{dx}{dt}$ and each $\frac{\partial\psi_j}{\partial x}\cdot\frac{dx}{dt}$ capture the phase and isostable coordinate dynamics when p is held constant. As such, these terms are identical to those from Eq. (9). The remaining terms can also be identified as described in [31] yielding the adaptive phase-isostable reduction

$$\dot\theta = \omega(p) + Z(\theta,p)(u-p) + D(\theta,p)\cdot\dot p,$$
$$\dot\psi_j = \kappa_j(p)\psi_j + I_j(\theta,p)(u-p) + Q_j(\theta,p)\cdot\dot p,$$
$$j = 1,\dots,\beta,$$
$$\dot p = G_p(p,\theta,\psi_1,\dots,\psi_\beta). \tag{13}$$

Above, $D(\theta,p)\in\mathbb{R}^M$ with the ith element is given by $-\frac{\partial x^\gamma}{\partial p_i}\cdot\frac{\partial\theta}{\partial x}$ where $\frac{\partial x^\gamma}{\partial p_i}|_{\theta_0,p} \equiv \lim_{a\to 0}(x^\gamma_{p+e_i a}(\theta_0) - x^\gamma_p(\theta_0))/a$, $\frac{\partial\theta}{\partial x}$ is evaluated in reference to x^γ_p, and e_i is the ith component of the standard unit basis. Likewise $Q_j(\theta,p)\in\mathbb{C}^M$ with the ith element given by $-\frac{\partial x^\gamma}{\partial p_i}\cdot\frac{\partial\psi_j}{\partial x}$ where $\frac{\partial\psi_j}{\partial x}$ is evaluated in reference to x^γ_p. Note that each ψ_j can potentially take complex values so that Q_j can also take complex values. When using Eq. (13) to represent the phase and isostable coordinate dynamics, Eq. (7) can be used to approximate the state. More details about this derivation are provided in [31].

The primary sources of error in the standard phase reduction (5) are associated with large deviations from the limit cycle and the application of large inputs relative to the baseline value. The variable p in Eq. (13) adds additional degrees of freedom that can mitigate these errors. For instance, provided G_p from Eq. (13) can be found so that $\psi_1(x,p),\dots,\psi_\beta(x,p)$ remain small, $x - x^\gamma_p$ will remain small, thereby limiting truncation errors that are associated with being perturbed far from an underlying limit cycle. General heuristics for the design of G_p are discussed in [31]. In a specific situation where only one isostable coordinate is necessary, $p\in\mathbb{R}^1$, and $Q_j(\theta,p)$ is bounded away from 0 for all θ and all allowable p, one can take

$$G_p = -\frac{I_1(\theta,p)}{Q_1(\theta,p)}(u-p), \tag{14}$$

so that the isostable coordinate dynamics follow $\dot\psi_1 = \kappa_1(p)\psi_1$ and hence can be ignored. This yields the resulting 2-dimensional reduction

$$\dot\theta = \omega(p) + Z(\theta,p)(u-p) - \frac{D(\theta,p)I_1(\theta,p)}{Q_1(\theta,p)}(u-p),$$
$$\dot p = -\frac{I_1(\theta,p)}{Q_1(\theta,p)}(u-p). \tag{15}$$

More generally, one can also use

$$G_p = -\nu\psi_1 Q(\theta,p), \tag{16}$$

where $\nu > 0$ so that the isostable coordinate dynamics become $\dot\psi_1 = (\kappa_1(p) - \nu Q^2(\theta,p))\psi_1 + I_1(\theta,p)(u-p)$. In this case, G_p effectively increases the decay rate of transients. Importantly, as explained in [31], the adaptive phase-isostable reduction strategy can be used to analyze the dynamics of (1) in a reduced order setting without placing limitations on the magnitude of the allowable inputs.

2.4. Operational phase coordinates

In much of this work, numerical approximations of infinitesimal phase and isostable response curves will be obtained using strategies similar to the direct method [2,9,10]. These strategies are implemented by applying a small input at a known initial phase and measuring the resulting changes in the phase and isostable coordinates. The asymptotic phase is relatively straightforward to measure by allowing the state to relax back to the limit cycle after the perturbation. Inference of isostable coordinates (that capture transient behavior) is more difficult necessitating the consideration of the operational phase described in [23]. This coordinate system distinguishes between asymptotic phase, θ, defined according to the isochrons (4) and an operational phase, θ^*, defined so that $\theta^*(x) = 0$ every time the state crosses a predefined Poincaré section.

The distinction between operational and asymptotic phase coordinates is necessary because it is generally not possible to precisely measure the asymptotic phase $\theta(x,p)$ for any $x\notin x^\gamma_p$. By contrast, the precise timing of the crossing of the $\theta^* = 0$ level set (i.e., Poincaré section) can always be determined once per cycle. As discussed in Appendix D, a number of relations are available that connect the operational phase to the asymptotic phase. For instance, the reduced order dynamics can be accurately captured using a single isostable coordinate ψ_1, to linear orders of accuracy

$$t^*_k = t_k - \frac{\psi_1(t_k)\alpha_1}{\omega(p)\kappa_1(p)}, \tag{17}$$

where t^*_k is the timing of the kth crossing of the $\theta^*(x,p) = 0$ level set, t_k is the timing of the kth crossing of the $\theta(x,p) = 0$ isochron, and α_1 is an arbitrary scale factor ($\alpha_1 = 1$ will be used in this work). Additionally, considering the Floquet eigenfunctions from Eq. (7),

$$g(0,p)\cdot n = \frac{x^{\gamma\prime}_p|_{\theta=0}\cdot n}{\kappa_1(p)}, \tag{18}$$

where $' \equiv d/d\theta$ and n is a unit vector normal to the Poincaré section used to define $\theta^* = 0$. Finally, as discussed in [23], features of the isostable coordinate dynamics can be inferred by considering an initial condition that has been perturbed from its limit cycle at x^γ_p. For instance, in the case where there is a single isostable coordinate, the associated Floquet exponent κ_1 can be obtained according to

$$\kappa_1(p) = \frac{\log(\tau_{n+1}/\tau_n)}{T(p)}, \tag{19}$$

where $\tau_i = t^*_{i+1} - t^*_i - T(p)$. Note that when noise is present, each τ_i used in the estimate of (19) must be taken soon after the initial perturbation; otherwise the measurement of τ_{n+1}/τ_n in Eq. (19) will be highly susceptible to the noise. Relations (17)–(19) will be used in conjunction with the proposed model identification strategy as described in Section 4. These equations are obtained directly from results presented in [23] as shown in Appendix D.

3. Inference of adaptive phase-isostable reduced models from first order accurate terms

The direct method [2,9,10] and related approaches [23,34] have been previously proposed to infer $Z(\theta,p)$ and $I_j(\theta,p)$ from (13) for a given x^γ_p by considering the phase response to pulsatile inputs. Ref. [35] suggests a similar strategy for finding $D(\theta,p)$ and each $Q_j(\theta,p)$ using step function inputs instead of pulses. Alternatively, the derivation presented below illustrates that the additional terms of the adaptive reduction $D(\theta,p)$ and $Q_j(\theta,p)$ are directly related to $Z(\theta,p)$ and $I_j(\theta,p)$, respectively. These relations are obtained by first considering the shift of the periodic orbit in response to a static perturbation using an isostable coordinate basis.

3.1. Response to static perturbations using an isostable coordinate basis

To begin, consider a periodic orbit $x_p^\gamma(\theta)$ of the general dynamical system (1) that results when holding u constant at the value p. Considering the solution in a basis of phase and isostable coordinates with dynamics governed by Eq. (9), the solution $\theta(t)$ and $\psi_j(t)$ in response to the static shift in input $u(t) = p+\epsilon e_i$ can be expanded in powers of ϵ where

$$\theta(t) = \theta_0(t) + \epsilon\theta_1(t) + \epsilon^2\theta_2(t) + \dots, \tag{20}$$

$$\psi_j(t) = \psi_{j,0}(t) + \epsilon\psi_{j,1}(t) + \epsilon^2\psi_{j,2}(t) + \dots, \tag{21}$$

for $j = 1, \dots, N-1$. First considering the solution $\theta(t)$, substituting Eq. (20) in to Eq. (9) yields

$$\dot\theta_0+\epsilon\dot\theta_1+\epsilon^2\dot\theta_2+\cdots = \omega+\epsilon Z^i(\theta_0(t)+\epsilon\theta_1(t)+\epsilon^2\theta_2(t)+\cdots, p), \tag{22}$$

where Z^i is the ith component of Z. Note that the dependence of ω on p has been suppressed for convenience of notation. Collecting $O(1)$ terms, $\dot\theta_0 = \omega$ so that $\theta_0(\omega t) = \theta(0) + \omega t$. For simplicity of exposition, let $\theta(0) = 0$. Continuing with the $O(\epsilon)$ terms

$$\dot\theta_1 = Z^i(\omega t, p), \tag{23}$$

so that

$$\theta_1(t) = \int_0^t Z^i(\omega s, p)ds + c_i, \tag{24}$$

where c_i is a constant to be determined momentarily. Next considering the isostable coordinates, substituting Eq. (21) into Eq. (9) yields

$$\dot\psi_{j,0} + \epsilon\dot\psi_{j,1} + \cdots = \kappa_j(\psi_{j,0}(t) + \epsilon\psi_{j,1}(t) + \dots) + \epsilon I_j^i(\theta_0(t) + \epsilon\theta_1(t) + \dots, p), \tag{25}$$

for $j = 1, \dots, N-1$ where I_j^i is the ith component of I_j. Once again, the dependence of κ_j on p has been suppressed for convenience of notation. Collecting $O(1)$ terms, $\dot\psi_{j,0} = \kappa_j\dot\psi_{j,0}$ so that $\psi_{j,0}(t) = \psi_{j,0}(0)\exp(\kappa_j t)$ and $\lim_{t\to\infty}\psi_j(t) = 0$. Continuing with the $O(\epsilon)$ terms

$$\dot\psi_{j,1} = \kappa_j\psi_{j,1} + I_j^i(\omega t, p) = \kappa_j\psi_{j,1} + b_{0,j}^i + \sum_{m=1}^{\infty}\left[a_{m,j}^i\sin(m\omega t) + b_{m,j}^i\cos(m\omega t)\right], \tag{26}$$

where the $a_{m,j}^i$ and $b_{m,j}^i$ are the Fourier series coefficients of $I_j^i(\omega t, p)$. After all transients have decayed Eq. (26) admits periodic solutions of the form

$$\psi_{j,1,ss}^i(t) = -\frac{b_{0,j}^i}{\kappa_j} + \sum_{m=1}^{\infty}\left[-\frac{a_{m,j}^i\kappa\sin(m\omega t)}{\kappa^2+\omega^2m^2} - \frac{a_{m,j}^i m\omega\cos(m\omega t)}{\kappa_j^2+\omega^2m^2} + \frac{b_{m,j}^i m\omega\sin(m\omega t)}{\kappa_j^2+\omega^2m^2} - \frac{b_{m,j}^i\kappa_j\cos(m\omega t)}{\kappa_j^2+\omega^2m^2}\right]. \tag{27}$$

With the above results in mind, next consider the expansions for $\theta(t)$ and $\psi_j(t)$ from Eqs. (20) and (21). For Eq. (20), to leading order ϵ

$$\theta(t) = \omega t + \epsilon\left[\int_0^t Z^i(\omega s, p)ds + c_i\right] + O(\epsilon^2), \tag{28}$$

After all transients have decayed, Eq. (21) becomes

$$\psi_{j,ss}^i(t) = \epsilon\psi_{j,1,ss}^i(t) + O(\epsilon^2). \tag{29}$$

Towards simplifying Eqs. (28) and (29) to find a periodic solution, let $G^i(\omega t, p) = Z^i(\omega t, p) - \bar Z^i(p)$, where $\bar Z^i(p) = \frac{1}{T}\int_0^T Z^i(\omega s, p)ds$. Eq. (28) can be rewritten as

$$\theta(t) = \omega_\Delta^i t + \epsilon\left(H^i(\omega t, p) + c_i\right) + O(\epsilon^2), \tag{30}$$

where $H^i(\omega t, p) = \int_0^t G^i(\omega s, p)ds$ and $\omega_\Delta^i = \omega + \epsilon\bar Z^i(p)$. Considering Eq. (7) which relates the phase and isostable coordinates to the state, substituting Eqs. (29) and (30) for the phase and isostable coordinates (which gives the solution after all transients have decayed), and neglecting $O(\epsilon^2)$ terms, the periodic solution resulting from the static shift in input is

$$x_{p+\epsilon e_i}^\gamma(\omega_\Delta^i t) = x_p^\gamma(\omega_\Delta^i t + \epsilon H^i(\omega t, p) + \epsilon c_i) + \sum_{j=1}^{N-1}\Big[\epsilon g_j\Big(\omega_\Delta^i t + \epsilon H^i(\omega t, p) + \epsilon c_i, p\Big)\psi_{j,1,ss}^i(\omega t)\Big]. \tag{31}$$

Taylor expanding x_p^γ and each g_j and $\psi_{j,ss}^i$ about $\omega_\Delta^i t$ from the above equation and neglecting $O(\epsilon^2)$ terms ultimately yields

$$x_{p+\epsilon e_i}^\gamma(\theta) = x_p^\gamma(\theta)+\epsilon x_p^{\gamma\prime}(\theta)(H^i(\theta, p)+c_i)+\sum_{j=1}^{N-1}\Big[\epsilon g_j(\theta, p)\psi_{j,1,ss}^i(\theta)\Big], \tag{32}$$

where $' \equiv d/d\theta$ and $\theta = \omega_\Delta t$ to leading order ϵ along the new periodic orbit. The constant shift c_i is related to the fact that each x_p^γ is unique up to a constant phase shift.

Eq. (32) gives an $O(\epsilon)$ accurate approximation for the shift in the periodic orbit in response to a static change in parameters. Note that Eq. (32) shares similarities with results from [39]. The advantage here is that working in an isostable coordinate basis allows for substantial simplification when considering the terms of the adaptive phase-isostable reduction from (12) as illustrated in Sections 3.2 and 3.3.

3.2. Inferring terms of the adaptive phase-isostable reduction with only pulse inputs

Considering Eq. (32) and the definition of $\frac{\partial x^\gamma}{\partial p_i}$ given under Eq. (13), one can write

$$\frac{\partial x^\gamma}{\partial p_i} = x_p^{\gamma\prime}(\theta)(H^i(\theta, p) + c_i) + \sum_{j=1}^{N-1}\Big[g_j(\theta, p)\psi_{j,1,ss}^i(\theta)\Big], \tag{33}$$

where θ is the asymptotic phase. Toward identification of the terms $D(\theta, p)$ and $Q_j(\theta, p)$ from the adaptive phase-isostable reduction (13), as discussed in [27], $\frac{\partial\theta}{\partial x}\cdot x_p^{\gamma\prime} = 1$ and $\frac{\partial\theta}{\partial x}\cdot g_j(\theta, p) = 0$ for all j, with all partial derivatives and functions evaluated at θ on the x_p^γ limit cycle. With this in mind, $D^i(\theta, p)$ can be written as

$$D^i(\theta, p) = -\frac{\partial x^\gamma}{\partial p_i}\cdot\frac{\partial\theta}{\partial x} = -H^i(\theta, p) - c_i. \tag{34}$$

Likewise, as discussed in [27], $\frac{\partial\psi_n}{\partial x}\cdot g_j(\theta, p) = 1$ if $j = n$ and 0 otherwise and $\frac{\partial\psi_n}{\partial x}\cdot x_p^{\gamma\prime} = 0$. Using this result in conjunction with Eq. (33) one finds

$$Q_j^i(\theta, p) = -\frac{\partial x^\gamma}{\partial p_i}\cdot\frac{\partial\psi_j}{\partial x} = -\psi_{j,1,ss}^i(\theta). \tag{35}$$

Recall from Eq. (27) that $\psi_{j,1,ss}^i(\theta)$ is fully specified by the Fourier coefficients of $I_j^i(\theta, p)$, ω, and κ_j; likewise, $H^i(\theta, p)$ is fully specified by $Z^i(\theta, p)$. As such, with the exception of c_i, the terms that comprise (34) and (35) are uniquely determined with knowledge of the first order accurate phase-isostable dynamics from (9). In determining the value of the constant c_i, recall that each $x_p^\gamma(\theta)$ is unique up to a constant phase shift in the implementation of

the adaptive phase–amplitude reduction (13). To disambiguate this constant phase shift, for instance, one can define a Poincaré section Σ as an $n-1$ dimensional hyperplane and take $\theta(x,p)=0$ to correspond to the intersection of Σ and x_p^γ for all p. With this definition, $x_p^\gamma \cdot n$ evaluated at $\theta = 0$ is constant, where n is a unit normal vector to Σ. Using this definition, starting with (32), taking the dot product with n on both sides and rearranging one finds

$$c_i = \frac{-\sum_{j=1}^{N-1}\left(\left(g_j(0,p)\cdot n\right)\psi_{j,ss}^i(0)\right) - \left(x_p^{\gamma\prime}(0)\cdot n\right)H^i(0,p)}{x_p^{\gamma\prime}(0)\cdot n}. \tag{36}$$

Above, $H(0,p)$ and each $\psi_{j,ss}(0)$ can be determined directly from the infinitesimal phase and isostable response curves. In applications where only one isostable coordinate is required, $g_j(0,p)\cdot n$ can be determined according to Eq. (18). As such, by inferring the first order accurate terms for a collection of periodic orbits that comprise (7) and (9), the necessary terms of the adaptive phase amplitude reduction from (13) are uniquely determined. Note that each D^i from Eq. (34) does not depend on the isostable coordinates and each Q_j^i from Eq. (35) only depends on the dynamics associated with the ψ_j isostable coordinate. As such, model order reduction that ignores the most rapidly decaying isostable coordinates is still possible when computing $D(\theta,p)$ and each necessary $Q_j(\theta,p)$ using a reduced order isostable coordinate basis.

3.3. Inferring terms of the adaptive phase-isostable reduction with only step function inputs

As discussed in [35] it is possible to infer the terms $D(\theta,p)$ and each $Q_j(\theta,p)$ from Eq. (13) using step function inputs. For instance, suppose $u(t) = p + \epsilon h(t_0)e_i$, where h is the Heaviside step function and e_i is the ith component of the standard unit basis. Using this step function input and letting $\dot{p} = e_i\delta(t_0)$ where δ is a delta function impulse, $u-p=0$ at all times. As such, by measuring the resulting change in the phase and isostable coordinates, i.e., $\Delta\theta$ and $\Delta\psi_j$, respectively, one can obtain pointwise estimate of $D^i(\theta(t_0),p) = \Delta\theta/\epsilon$ and $Q_j^i(\theta(t_0),p)/\epsilon$. This process can be repeated for multiple values of $\theta(t_0)$ and subsequently for different initial values of p allowing $D(\theta,p)$ and each $Q_j(\theta,p)$ to be fit to the resulting data.

Considering the results from Sections 3.1 and 3.2, it is also possible to apply a series of step function inputs to infer $D(\theta,p)$ along with each $Q_j(\theta,p)$ and subsequently compute $Z(\theta,p)$ and each $I_j(\theta,p)$. Starting with the inference of the infinitesimal phase response curve, $Z(\theta,p)$, consider Eq. (34) after substituting $\theta = \omega t$ along the limit cycle:

$$\begin{aligned} D^i(\omega t,p) &= -H^i(\omega t) - c_i, \\ &= \int_0^t -Z^i(\omega s,p) + \bar{Z}^i(p)ds - c_i. \end{aligned} \tag{37}$$

Taking the time derivative and rearranging yields

$$Z^i(\omega t,p) = -\frac{d}{dt}\left(D^i(\omega t,p)\right) + \bar{Z}^i(p). \tag{38}$$

As discussed elsewhere [39], to leading order the shift in frequency is directly related to the average value of the infinitesimal phase response curve, i.e., $\bar{Z}^i(p) \approx (\omega(p+\epsilon e_i)-\omega(p))/\epsilon$. Thus, an estimate of $Z(\theta,p)$ from (13) can be obtained with knowledge of both $D(\theta,p)$ and the shift in the natural frequency resulting from a static shift in the parameters.

Next, for inference of the infinitesimal isostable response curves, letting $Q_j^i(\theta,p) = \beta_{0,j}^i + \sum_{m=1}^\infty \left[\alpha_{m,j}^i \sin(m\theta) + \beta_{m,j}^i \cos(m\theta)\right]$ where $\alpha_{m,j}^i$ and $\beta_{m,j}^i$ are Fourier coefficients of $Q_j^i(\theta,p)$, and considering Eq. (35), after algebraic manipulation one finds

$$\begin{aligned} &\beta_{0,j}^i + \sum_{m=1}^\infty \left[\alpha_{m,j}^i \sin(m\theta) + \beta_{m,j}^i \cos(m\theta)\right] \\ &= -\psi_{j,ss}^i \\ &= \frac{b_{0,j}^i}{\kappa_j} + \sum_{m=1}^\infty \left[\frac{a_{m,j}^i \kappa \sin(m\theta)}{\kappa^2+\omega^2m^2} + \frac{a_{m,j}^i m\omega\cos(m\theta)}{\kappa^2+\omega^2m^2}\right. \\ &\quad \left. - \frac{b_{m,j}^i m\omega \sin(m\theta)}{\kappa^2+\omega^2m^2} + \frac{b_{m,j}^i \kappa\cos(m\theta)}{\kappa^2+\omega^2m^2}\right], \end{aligned} \tag{39}$$

where the final line is obtained using Eq. (27). Subsequently, equating Fourier coefficients in Eq. (39) yields

$$\begin{aligned} b_{0,j}^i &= \beta_{0,j}^i\kappa_j, \\ \begin{bmatrix} a_{m,j}^i \\ b_{m,j}^i \end{bmatrix} &= \begin{bmatrix} \kappa & m\omega \\ -m\omega & \kappa \end{bmatrix} \begin{bmatrix} \alpha_{m,j}^i \\ \beta_{m,j}^i \end{bmatrix}. \end{aligned} \tag{40}$$

Recall here that a_k and b_k are the Fourier series coefficients of $I_j^i(\theta)$ as defined below Eq. (26). Eq. (40) provides a direct relationship between the Fourier coefficients of $Q_j^i(\theta,p)$ and the Fourier coefficients of $I_j^i(\theta,p)$ from Eq. (13).

3.4. Summary of analytical results

In summary, the adaptive phase-isostable reduction from Eq. (13) is comprised of terms from the first order accurate phase-isostable reduction from Eq. (9) (i.e., $\omega(p)$, $Z(\theta,p)$, and both $I_j(\theta,p)$ and $\kappa_j(p)$ for each nontruncated isostable coordinate) along with the terms $D(\theta,p)$ and $Q_j(\theta,p)$ for each nontruncated isostable coordinate. As illustrated in the previous sections, the terms $D(\theta,p)$ and $Q_j(\theta,p)$ can be computed explicitly with knowledge of $\omega(p)$, $Z(\theta,p)$, $I_j(\theta,p)$, and $\kappa_j(p)$. Additionally, $Z(\theta,p)$ and $I_j(\theta,p)$ can be computed explicitly with knowledge of $\omega(p)$, $D(\theta,p)$, $Q_j(\theta,p)$, and $\kappa_j(p)$. As such, a direct method approach for the computation of these necessary terms can be implemented in one of the following two ways:

(1) Using pulsatile inputs, the resulting changes to the phase and isostable coordinates can be inferred using strategies similar to the direct method [23,34]. Subsequently, $Z(\theta,p)$ and each $I_j(\theta,p)$ with associated $\kappa_j(p)$ can be determined for a collection of periodic orbits x_p^γ. The remaining terms $D(\theta,p)$ and each $Q_j(\theta,p)$ can be determined according to Eqs. (34) and (35), respectively.
(2) Using step function inputs the resulting changes to the phase and isostable coordinates can be inferred using strategies similar to the direct method [23,34]. Subsequently, $D(\theta,p)$ and each $Q_j(\theta,p)$ with associated $\kappa_j(p)$ can be determined for a collection of periodic orbits x_p^γ. The remaining terms $Z(\theta,p)$ and each $I_j(\theta,p)$ can be determined according to Eqs. (38) and (40), respectively.

When using either strategy 1 or 2 above, $\omega(p)$ can be inferred from the unperturbed natural period. Fig. 2 provides a schematic reasoning for the theoretical results from Section 3.

The computational results to follow in Section 4 illustrate both of these model identification approaches for a collection of numerical models. Results from Sections 4.2 and 4.3 use strategies 1 and 2, respectively, but either strategy could be implemented in both of these applications.

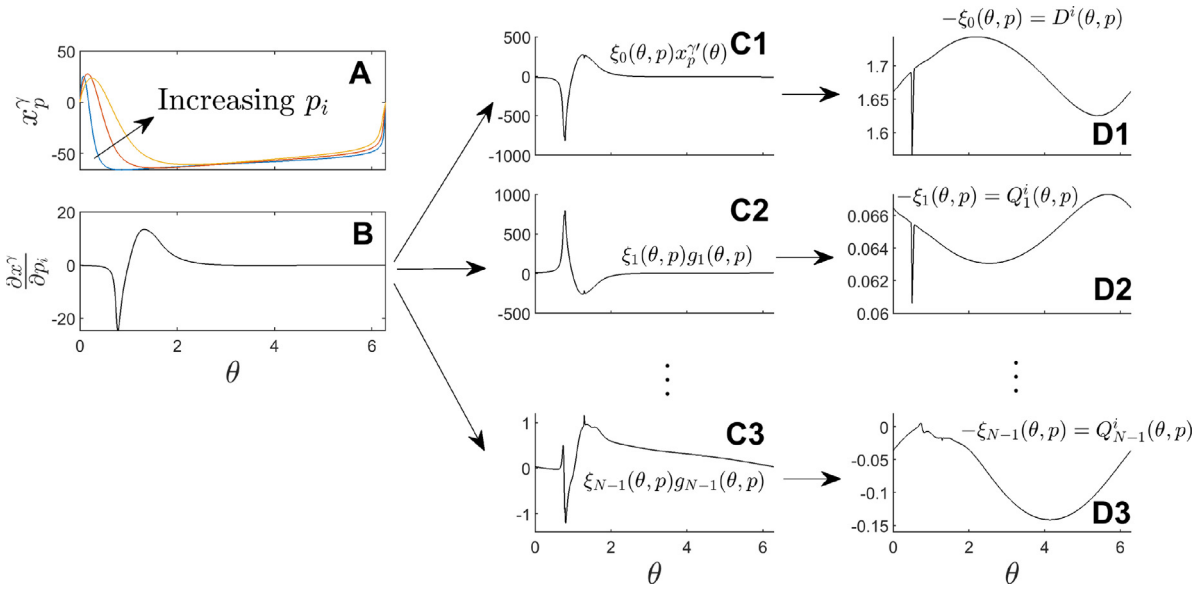

Fig. 2. A schematic reasoning for the theoretical results from Section 3. For a general dynamical system with a stable limit cycle x_p^γ, the shape of the limit cycle will change with static shifts to the parameter p_i (Panel A). In the limit that the change in the parameter p_i is small, the change in the periodic orbit is proportional to $\frac{\partial x^\gamma}{\partial p_i}$ (Panel B). At all values of θ, $\frac{\partial x^\gamma}{\partial p_i}$ can be decomposed as a linear combination of $x_p^{\gamma\prime}(\theta)$, $g_1(\theta,p),\ldots,g_{N-1}(\theta,p)$ (panels C1 through C3). The resulting coefficients of this linear combination. $\xi_0(\theta,p),\ldots,\xi_{N-1}(\theta,p)$, are directly related to the terms $D^i(\theta,p)$, $Q_1^i(\theta,p),\ldots,Q_{N-1}^i(\theta,p)$ (Panels D1 through D3). Ultimately, as shown in Section 3, the coefficients $\xi_0(\theta,p),\ldots,\xi_{N-1}(\theta,p)$ can be computed with knowledge of the terms that comprise the phase-isostable reduction of the form (9).

4. Numerical illustration

4.1. Illustration in a simple dynamical model with an analytical solution

The derived relationships (34), (35), (38), and (40) are illustrated for a simple dynamical model

$$\begin{aligned}\dot{x}&=\sigma x(\mu^2(t)-r^2)-y(1+\eta(r^2-\mu^2(t))),\\ \dot{y}&=\sigma y(\mu^2(t)-r^2)+x(1+\eta(r^2-\mu^2(t))).\end{aligned}\tag{41}$$

Here, x and y are state variables representing Cartesian coordinates, $r=x^2+y^2$, σ and η are model parameters, and μ is a bifurcation parameter. Stable oscillations emerge resulting from a Hopf bifurcation when taking $\mu>0$. Here, μ will also be considered as a control input. For constant values of μ, Eq. (41) admits stable periodic solutions $x_\mu^\gamma(t)=[\mu\cos(t),\mu\sin(t)]^T$. Because Eq. (41) is two-dimensional, each periodic orbit has one isostable (amplitude) coordinate. Analytic solutions for the reduced order equations associated with Eq. (41) can be obtained as described below.

To begin, the gradient of the phase can be obtained by finding appropriately normalized periodic solutions of the adjoint Eq. (C.1). For this model, these solutions are $[d\theta/dx,d\theta/dy]=[\eta\cos(t)/\sigma\mu-\sin(t)/\mu,\eta\sin(t)/\sigma\mu+\cos(t)/\mu]$. Additionally, $\frac{\partial F}{\partial\mu}=[2\mu^2(\eta\sin(t)+\sigma\cos(t)),2\mu^2(\sigma\sin(t)-\eta\cos(t))]^T$. Directly computing the infinitesimal phase response curve using the relation provided just below Eq. (5),

$$Z(\theta,\mu)=\left[\frac{d\theta}{dx},\frac{d\theta}{dy}\right]\frac{\partial F}{\partial\mu}=0.\tag{42}$$

Furthermore, $\frac{\partial x_\mu^\gamma}{\partial\mu}=[\cos(t),\sin(t)]^T$ so that using the relation provided just below Eq. (13)

$$D(\theta,\mu)=-\frac{\partial x^\gamma}{\partial\mu}^T\left[\frac{d\theta}{dx},\frac{d\theta}{dy}\right]=-\frac{\eta}{\mu\sigma}.\tag{43}$$

Notice that Eq. (38) holds for $Z(\theta,\mu)$ and $D(\theta,\mu)$ above, i.e., that $\frac{dD}{dt}=0$ so that $Z(\theta,\mu)$ must be a constant. Because the frequency does not depend on μ, the right hand side of Eq. (38) is zero yielding the correct infinitesimal phase response curve. Similarly, it is straightforward to verify that Eq. (34) holds here.

Continuing for the isostable coordinate dynamics, in radial coordinates, Eq. (41) becomes

$$\begin{aligned}\dot{r}&=\sigma(\mu(t)^2-r^2)r,\\ \dot{v}&=1+\eta(r^2-\mu(t)^2),\end{aligned}\tag{44}$$

where $v=\arctan(y/x)$. These radial dynamics are decoupled from the angular dynamics with the analytical solution.

$$r(t)=\frac{\mu\exp(\mu^2(\alpha_1+\sigma t))}{\sqrt{\exp(2\mu^2(\alpha_1+\sigma t))+1}},\tag{45}$$

valid for $\mu>0$ where α_1 is a constant determined by the initial condition. In the limit as time approaches infinity, Eq. (45) is well approximated by $r(t)-\mu=\alpha_2\exp(-2\mu^2\sigma t)$ where α_2 is a constant that depends on initial conditions. As such, the Floquet exponent is $\kappa_1(\mu)=-2\mu^2\sigma$. Eq. (C.2) admits periodic solutions of the form $[d\psi_1/dx,d\psi_1/dy]=[\cos(t),\sin(t)]$. Taking $\mu(t)$ as the input, one finds

$$\begin{aligned}I_1(\theta,\mu)&=\left[\frac{d\psi_1}{dx},\frac{d\psi_1}{dy}\right]\frac{\partial F}{\partial\mu}=2\mu^2\sigma,\\ Q_1(\theta,\mu)&=-\frac{\partial x^\gamma}{\partial\mu}^T\left[\frac{d\psi_1}{dx},\frac{d\psi_1}{dy}\right]=-1,\end{aligned}\tag{46}$$

where I_1 is defined below Eq. (9) and Q_1 is defined below Eq. (13). Once again, the relationship (40) mandates that $I_1(\theta,\mu)=-\kappa_1=2\mu^2\sigma$ as expected. It is also straightforward to verify that Eq. (35) holds. With knowledge of the terms of the adaptive reduction, one can use (15) to represent Eq. (41) as

$$\begin{aligned}\dot{\theta}&=1+2\eta p(p-\mu(t)),\\ \dot{p}&=2p^2\sigma(\mu(t)-p).\end{aligned}\tag{47}$$

Notice that Eq. (47) shares similarities with the polar form of the model Equations from (44), but is not identical.

Fig. 3 gives a comparison between the adaptive model from (47) and the phase-isostable-based model of the form (9). Note

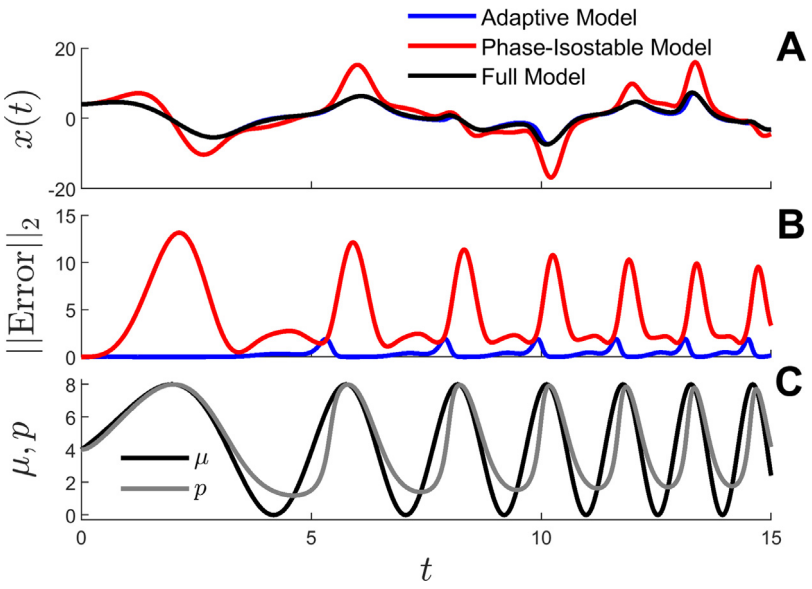

Fig. 3. Simulations of the simple model from (41) are compared to the adaptive model equations (47) and the phase-isostable-based Eqs. (9). Panel A shows traces of $x(t)$ in response to the input $\mu(t)$ from panel C. The corresponding 2-norm of the error is shown in panel B. Panel C also compares the parameter, p, to the actual input, μ, over the course of the simulation.

neither of these are reduced order models since the dimension of each is still two. Outputs of each transformed model are approximated according to (7). The terms of the phase-isostable reduction are computed according to their values for $\mu = 4$. Panel A of Fig. 3 shows the state $x(t)$ in response to the input $\mu(t) = 4 + 4\sin(0.5t + 0.15t^2)$. Panel B shows the corresponding error as the 2-norm of $[x(t) - \hat{x}(t), y(t) - \hat{y}(t)]$ where $x(t)$ and $y(t)$ is the output from the true model equations (41) and $\hat{x}(t)$ and $\hat{y}(t)$ are the approximations from the indicated model. The adaptive model agrees much better with the true model simulations. Panel C compares the input $\mu(t)$ to the value of $p(t)$ for the adaptive model. Results are qualitatively similar when using different inputs of similar magnitude (not shown).

4.2. Illustration in a noisy model of a tonically firing neuron

Here, the proposed model identification algorithm is illustrated using the Wang–Buzsaki model of neural spiking behavior [40],

$$\begin{aligned} C\dot{V} &= -g_{\text{Na}} m_\infty^3 h(V - E_{\text{Na}}) - g_{\text{K}} n^4 (V - E_K) - g_{\text{L}}(V - E_{\text{L}}) \\ &\quad - i_w + i_{\text{b}}(t) + \sqrt{2\zeta}\,\chi(t), \\ \dot{h} &= \gamma\,[\alpha_h(V)(1-h) - \beta_h(V)h], \\ \dot{n} &= \gamma\,[\alpha_n(V)(1-n) - \beta_n(V)n], \\ \dot{w} &= a(1.5/(1+\exp((b-V)/k)) - w). \end{aligned} \tag{48}$$

Above, V represents the transmembrane voltage, h and n are gating variables, $i_{\text{b}}(t)$ is a baseline current (in $\mu\text{A/cm}^2$), and $\sqrt{2\zeta}\,\chi(t)$ is zero-mean Gaussian noise with intensity $\zeta = 0.2$. Here, the dynamical equations have been augmented with an adaptation current [41], $i_w = g_w w(V - E_{\text{K}})$ where $g_w = 2\ \text{mS/cm}^2$ and $E_k = -90$ mV. A full description of the model equations and parameters is given in Appendix A.

The baseline current i_{b} is taken to be an input. Writing Eq. (48) in the same form as Eq. (10) yields $U_e(x, i_{\text{b}}(t), p) = \begin{bmatrix}(i_{\text{b}}(t) - p) & 0 & 0 & 0\end{bmatrix}^T$ where $x = \begin{bmatrix}V & h & n & w\end{bmatrix}^T$. For constant values of $i_b \in [4, 20]\ \mu\text{A/cm}^2$, the neuron is in a periodically firing regime with period $T \in [3.8, 14.3]$. Here, larger baseline currents correspond to shorter unperturbed periods. For any x on the periodic orbit $x^\gamma_{i_b}$, an action potential is defined to occur at the moment the transmembrane potential crosses 0 with a positive slope. Here, the crossing of this $V = 0$ Poincaré section is taken to correspond to the $\theta = 0$ level set for all periodic orbits.

4.2.1. Direct method inference of infinitesimal phase and isostable response curves using pulsatile inputs

A model of the form (13) with a single isostable coordinate will be inferred from noisy simulations of (48) using a slight modification of the direct method [9,10] to compute $Z(\theta, i_b)$, $\kappa(i_b)$, and $I_1(\theta, i_b)$ associated with $x^\gamma_{i_b}$ for $i_b \in [4, 20]$. This approach employs an operational phase–amplitude coordinate system [23]. For a given choice of θ_0 and i_0 pulse inputs of the form

$$i_b(t) = \begin{cases} i_0 + \Delta i, & t_s + \theta_0 \frac{T(i_0)}{2\pi} < t < t_s + \theta_0 \frac{T(i_0)}{2\pi} + \Delta t \text{ and} \\ & t_s < t_{\max}, \\ i_0, & \text{otherwise}, \end{cases} \tag{49}$$

are applied where t_s denotes the timing of the most recent action potential, Δi corresponds to the magnitude of a pulse input lasting Δt time units, and $t_{\max}$ sets the duration of series of pulse trains. Fig. 4 highlights the pulsing protocol mandated by Eq. (49). Assume that $t_{\max}$ is chosen to be large enough so that the effect of initial conditions dies out, during the application of pulse inputs kth interspike interval will be

$$\begin{aligned} t^*_{k+1} - t^*_k &= t_{k+1} - t_k - \frac{\alpha_1}{\omega\kappa_1}(\psi_1(t_{k+1}) - \psi_1(t_k)) \\ &= t_{k+1} - t_k. \end{aligned} \tag{50}$$

Derivation of the above equation uses Eq. (17) along with the fact that $\psi_1(t_{k+1}) = \psi_1(t_k)$ in steady state. As such, the kth interspike interval corresponds to the time between subsequent crossings of the $\theta = 0$ isochron. Note that in the above equation, the dependence of κ_1 and ω on i_0 is suppressed for convenience of notation. Considering the form of the reduced order Eq. (13) with $p = i_0$ held constant, in steady state, the change in phase resulting from the pulse occurring on each cycle is well approximated by $\Delta\theta \approx Z(\theta_0, i_0)\Delta i \Delta t$. The difference in the interspike interval will be $t^*_{k+1} - t^*_k = t_{k+1} - t_k = T(i_0)(1 - \Delta\theta/2\pi)$ so that a pointwise estimation of the infinitesimal phase response curve can be obtained according to

$$Z(\theta_0, i_0) \approx -\frac{2\pi}{T(i_0)\Delta i \Delta t}(dt^* - T(i_0)), \tag{51}$$

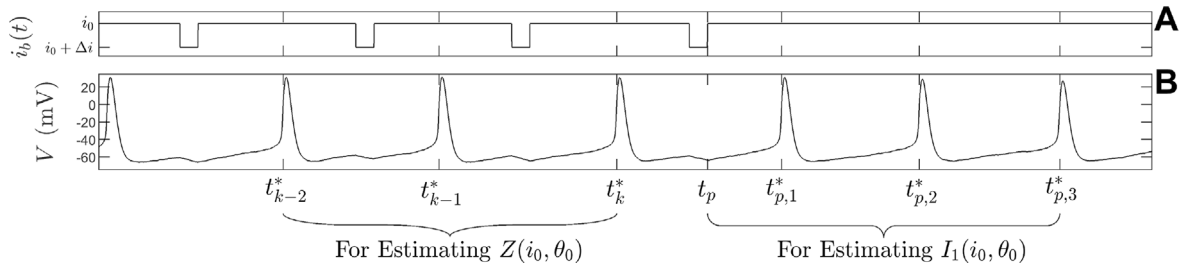

Fig. 4. Illustration of the pulsing protocol from Eq. (49) used to obtain estimates of $Z(\theta_0, i_0)$ and $I_1(\theta_0, i_0)$. A series of pulses are applied for $t < t_{\max}$ with the last pulse being applied at t_p. Action potentials that occur before t_p are used to obtain a pointwise estimate of $Z(\theta_0, i_0)$ according to Eq. (51). Action potentials that occur after t_p are used to obtain a pointwise estimate of $I_1(\theta_0, i_0)$ according to Eq. (55). This procedure is repeated for multiple values of θ_0 and i_0 and the infinitesimal phase and isostable response curves are fit to the data.

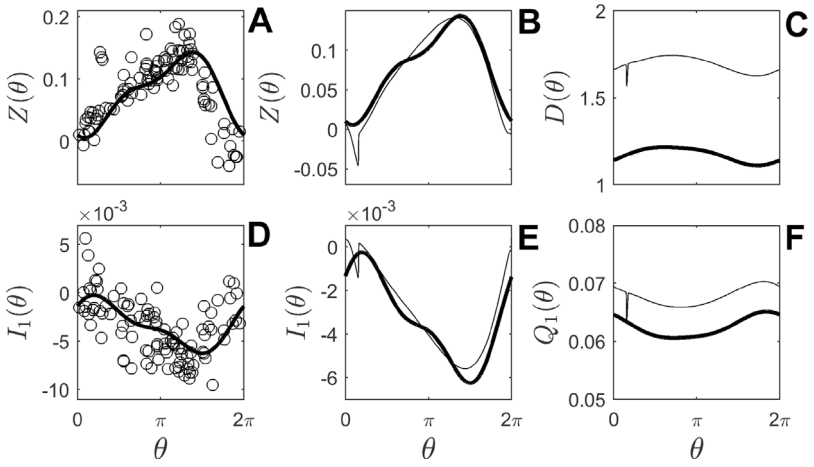

Fig. 5. Terms of the adaptive phase-isostable reduction from Eq. (13) for the $x^{\gamma}_{i_b}$ periodic orbit taking $i_b = 12$ μA/cm^2. Open circles in panels A and D are obtained according to Eqs. (51) and (55), respectively. Infinitesimal phase and isostable response curves are fit using a Fourier series basis and shown as solid lines. Panels B and E compare the Fourier series fits to the data (thick black lines) to the true infinitesimal phase and isostable response curves (thin black lines) obtained from periodic solutions to Eqs. (C.1) and (C.2), respectively. Panels C and F show $D(\theta)$ and $Q(\theta)$ inferred from relations given in Section 3.2 using the infinitesimal phase and isostable response curves obtained from the direct method (thick black lines). These are compared to the true values (thin black lines).

where $dt^* = \frac{1}{N}\sum_{k=1}^{N}\left(t^*_{k+1} - t^*_k\right)$ is taken as the average of the N preceding interspike intervals in order to average out the effects of noise. To infer pointwise estimates of the infinitesimal isostable response curve, one can consider the decay back to the limit cycle after the pulses stop. Letting t_p be the moment immediately after the final pulse is applied, as discussed in [23], each subsequent action potential occurs when

$$2\pi n = \theta^*(t_p) + \omega(t^*_{p,n} - t_p) + \frac{\psi(t_p)}{\kappa_1}\exp(\kappa_1(t^*_{p,n} - t_p) - 1), \quad (52)$$

is satisfied, where $t^*_{p,n}$ is the nth spike after the final pulse input is applied. Comparing the first and the nth spikes after the final pulse is applied, one finds

$$\psi_1(t_p) = \frac{\kappa_1\left(2\pi(n-1) - \omega(t^*_{p,n} - t^*_{p,1})\right)}{\exp(\kappa_1(t^*_{p,n} - t_p)) - \exp(\kappa_1(t^*_{p,1} - t_p))}. \quad (53)$$

Once again, considering the isostable coordinate dynamics of the reduced order Eq. (13) with $p = i_0$ held constant, immediately after each pulse is applied,

$$\psi_1(t_p) \approx I_1(\theta_0, i_0)\Delta i \Delta t + \psi_1(t_p)\exp(\kappa_1 dt^*), \quad (54)$$

where approximate equality comes from the fact that the effect of initial transients have died out so that the isostable coordinate immediately preceding the previous pulse is identical to $\psi_1(t_p)$ and dt^* is used in order to average out the effects of noise. Rearranging yields pointwise estimates of the infinitesimal isostable response curve

$$I_1(\theta_0, i_0) \approx \frac{\psi_1(t_p)(1 - \exp(\kappa_1 dt^*))}{\Delta i \Delta t}, \quad (55)$$

where $\psi_1(t_p)$ is computed according to from Eq. (53). Finally, as discussed in [23] using the same time series data, a representative estimate of $\kappa_1(p)$ can be obtained according to (19).

4.2.2. Reduced order model validation

Infinitesimal phase response curves are approximated according to the strategy described in Section 4.2.1 taking $i_b \in [4, 20]$ μA/cm^2. Results are shown in Fig. 5 for the curves obtained for the $x^{\gamma}_{i_b}$ periodic orbit taking $i_b = 12$ μA/cm^2. Open circles in panels A and D are obtained according to Eqs. (51) and (55), respectively. The spread in the data is a result of the Gaussian noise in the system Eqs. (48). This data is fit to the Fourier series basis $\sum_{n=0}^{2}[a_n \sin(n\theta) + b_n \cos(n\theta)]$ with resulting curves shown in black. Panels B and E compare these Fourier series fits to the infinitesimal phase and isostable response curves obtained using the adjoint method of solution described in Appendix C. Note that the adjoint equations are solved taking the noise intensity to be $\zeta = 0$ and represent the true values of the infinitesimal phase and isostable response curves. The thick black line in Panel C (resp., panel F) shows the value of $D(\theta)$ (resp., $Q_1(\theta)$) inferred according to Eq. (34) (resp., Eq. (35)) using the data obtained from the direct method. Thin black lines in panels C and F are computed directly according to the relations given under Eq. (13). The curves obtained according to the direct method accurately identify low frequency components of each curve. The Floquet exponent associated with these curves is inferred using Eq. (19) to be $\kappa_1(12) = -0.054$ compared to the true value of -0.042. This mismatch ultimately contributes to the

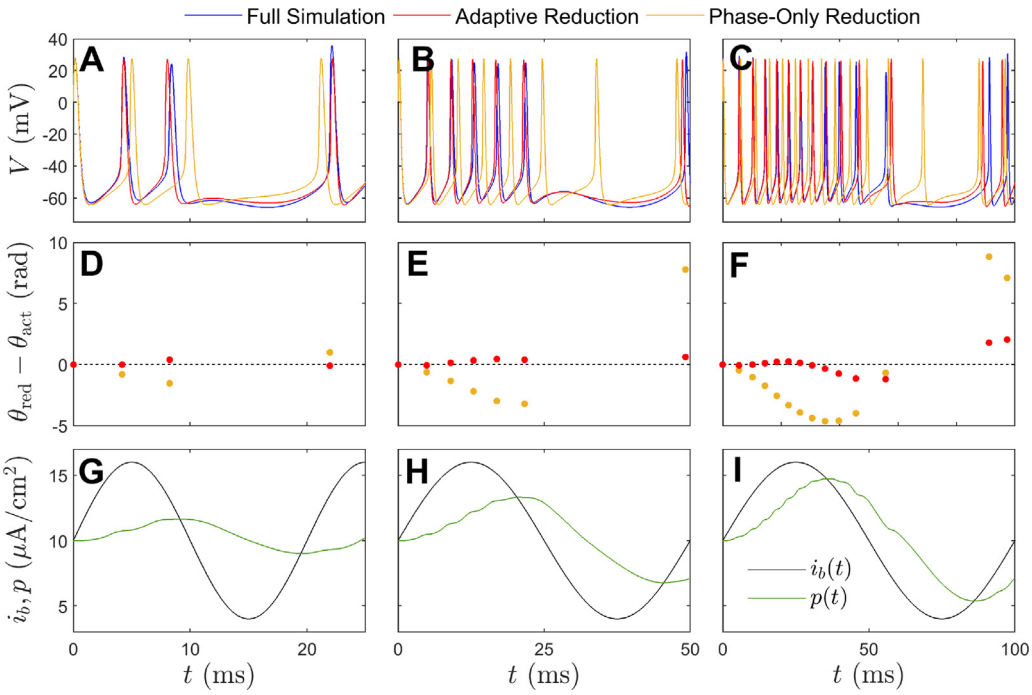

Fig. 6. Panels A, B, and C compare transmembrane voltage outputs for the full neural model simulation from Eq. (48) (blue), adaptive reduction (red), and phase-only reduction (yellow) in response to the inputs $i_b(t)$ from panels G, H, and I, respectively. Panels D, E, and F show the error between these full and reduced order simulations over time. The horizontal dashed line at $\theta_{\text{red}} - \theta_{\text{act}} = 0$ is shown for reference. Green lines in panels G, H, and I show traces of the adaptive parameter $p(t)$ over the course of simulations of the adaptive reduction. For slower varying inputs, the adaptive parameter $p(t)$ follows $i_b(t)$ more closely.

vertical offset between the true curves and the curves obtained from noisy data. Results shown in Fig. 5 are representative of the results obtained when taking different constant values for periodic orbits $x^{\gamma}_{i_b}$ for different choices of i_b. Despite the fact that the direct method does not perfectly identify the terms comprising the adaptive phase-isostable reduced order Eqs. (13), the resulting model still accurately captures the response to general inputs as shown in the results below.

Outputs from both the adaptive phase-isostable reduction from Eq. (13) and the phase-only reduction of the form (5) are compared to full model simulations using sinusoidal inputs with different frequencies. Results are shown in Fig. 6. For the adaptive reduction, the update rule $\dot{p} = G_p(i_b, \theta, \psi_1) = -1000(Q_1(\theta, i_b)\psi_1)$ and is of the same form as (16). The output $V(t)$ is taken to be $V^{\gamma}_p(\theta(t))$, that is, the voltage corresponding to $\theta(t)$ on the x^{γ}_p periodic orbit. The phase-only reduction uses infinitesimal phase response curves associated with the periodic orbit that results when taking $i_b = 10$ μA/cm^2. Panels A, B, and C, show the transmembrane voltage output for each model and panels D, E, and F show the resulting difference between the phase from the reduced order model, θ_{red}, and the full order simulation, θ_{act}, in response to the inputs $i_b(t)$ in panels G, H, and I, respectively. Note that panels D, E, and F, only show discrete measurements because the phase of the full order simulations can be measured once per cycle when the neuron fires an action potential (thereby crossing the $\theta = 0$ level set). Also, while the reduced order models were inferred using noisy data, the simulations from Fig. 6 take the noise intensity to be $\zeta = 0$ in order to compare the accuracy of the reduced order and full order models without the confounding influence of noise. For each of the trials shown in Fig. 6 the adaptive reduction accurately reflects the timing of action potentials for the full order model while the accuracy of the phase-only model tends to degrade over time.

4.3. Illustration in a model for the mammalian circadian clock

Here, the proposed model identification strategy is illustrated for a 16-dimensional computational model for the mammalian circadian clock comprised of interacting regulatory loops associated with Per, Cry, Bmal1 and Clock genes [42]. Full dynamical equations are given in Appendix B. The influence of light is included by modulating v_{sP}, which sets the maximum the rate of Per expression; v_{sP} is chosen as the input in the implementation of the adaptive phase-isostable reduction (13). Here, $v_{sP} = 1.2$ nM/h is considered a state of total darkness and $v_{sP} = 1.8$ nM/h corresponds to a maximum level of brightness. Colored lines in Panel A of Fig. 7 shows periodic orbits that result for values $v_{sP} \in [1.2, 1.6]$. Note that while the full model has 16 state variables, only the mRNA concentrations of Per, Cry and Bmal1 (M_P, M_C, and M_B, respectively) are plotted here. Each periodic orbit has an unperturbed period $T(v_{sP}) \in [23.7, 24.2]$. In panel A the black line shows an example trajectory starting on the periodic orbit that results when taking $v_{\text{sP}} = 1.2$ nM/h. Over the course of the simulation, v_{sP} is elevated to 1.8 nM/h for a duration of 60 h. The resulting trajectory quickly leaves the vicinity of the $v_{\text{sP}} = 1.2$ nM/h orbit, traveling closer to other orbits over the course of the simulation. Panels B and C highlight that the response of the phase and isostable coordinate to small step function perturbations is substantially different for each orbit indicating that the standard first order accurate phase reduction (5) will be unable to accurately capture the effects of these inputs.

For implementation of the adaptive phase-isostable reduced Eqs. (13), $\theta = 0$ for each orbit corresponds to the moment that the trajectory crosses Poincaré section for which $M_P = 1$ nM with a positive slope. Methods from [23] can be used to infer the terms $D(\theta, v_{sP})$ and $Q_1(\theta, v_{sP})$ from time series data assuming that traces of $M_P(t)$ can be accurately recorded. Note that this model

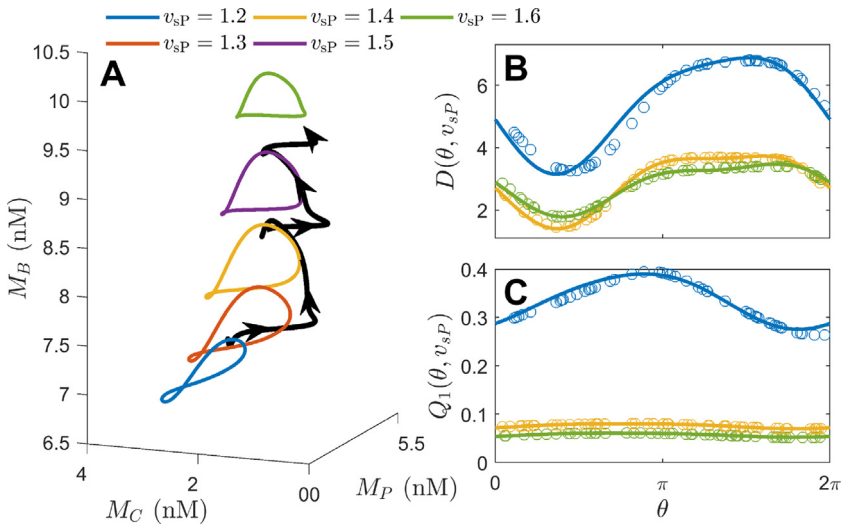

Fig. 7. Colored traces in Panel A show periodic orbits $x^{\gamma}_{v_{sP}}$ that emerge for different choices of v_{sP} (in nM/h). The black line highlights a trajectory starting from an initial condition on the $v_{sP} = 1.2$ nM/h orbit and subsequently elevating v_{sP} to 1.8 nM/h for 60 h. The perturbed trajectory does not stay close to any single orbit over the course of the simulation. Panels B and C illustrate how $D(\theta, v_{sP})$ and $Q_1(\theta, v_{sP})$ change for different periodic orbits color coded according to the associated value of v_{sP}. The dots represent individual approximations using the direct method calculated according to Eqs. (57) and (58) and this data is fit to a Fourier series basis.

identification procedure could be implemented using a different observable provided the Poincaré section that defines $\theta = 0$ is defined appropriately.

4.3.1. Direct method inference of reduced order model terms using step function inputs

A model of the form (13) with a single isostable coordinate will be inferred from simulations of the circadian model from Appendix B in response to step function inputs. In contrast to the previous example, $D(\theta, v_{sP})$ and $Q_1(\theta, v_{sP})$ will be approximated using the direct method and subsequently used to infer the terms of $Z(\theta, v_{sP})$ and $I_1(\theta, v_{sP})$ according to Eqs. (38) and (40), respectively. To implement the direct method, consider an initial state $x_0 \in x^{\gamma}_{v_{sP,0}}$ with a phase $\theta(x_0, v_{sP,0}) = \theta_0$. Such an initial condition can be obtained by holding v_{sP} at $v_{sP,0}$ long enough for transients to decay. Letting

$$v_{sP}(t) = v_{sP,0} + h(t_p)\Delta p, \tag{56}$$

where $h(t)$ is the Heaviside step function, the curve $D(\theta_0, v_{sP,0})$ can be approximated according to

$$D(\theta_0, v_{sP,0}) \approx \frac{2\pi n - \theta_0 - \omega(t^*_{p,n} - t_p)}{\Delta p}, \tag{57}$$

where $t^*_{p,i}$ is the ith crossing of the Poincaré section that defines $\theta = 0$ after step function input is applied. In Eq. (57), n must be chosen large enough so that $x(t^*_{p,n})$ is close to $x^{\gamma}_{v_{sP,0}+\Delta p}$. Likewise, with the approximation $Q_1(\theta, v_{sP,0}) \approx \Delta\psi_1/\Delta p$ and considering Eq. (53), one finds

$$Q_1(\theta, v_{sP,0}) \approx \frac{\kappa_1(2\pi(n-1) - \omega(t^*_{p,n} - t^*_{p,1}))}{\Delta p(\exp(\kappa_1(t^*_{p,n} - t_p)) - \exp(\kappa_1(t^*_{p,1} - t_p)))}. \tag{58}$$

Note that in Eqs. (57) and (58), κ_1 and ω correspond to the Floquet exponent and natural frequency associated with the $x^{\gamma}_{v_{sP,0}+\Delta p}$ orbit. These equations can be used to provide pointwise approximations for $D(\theta, p)$ and $Q_1(\theta, p)$ and a periodic function can be fit to the data. For each trial using the step function input from (56), an estimate of $\kappa_1(v_{sP,0}+\Delta p)$ can be obtained according to Eq. (19) by considering the relaxation to the periodic orbit $x^{\gamma}_{v_{sP,0}+\Delta p}$ after the step function input that occurs at t_p.

4.3.2. Reduced order model validation

Eqs. (57) and (58) are used to approximate $D(\theta, v_{sP})$ and $Q_1(\theta, v_{sP})$ with results shown as open circles in panels B and C of Fig. 7. Associated infinitesimal phase and isostable response curves are inferred using Eqs. (38) and (40) and shown as solid lines in Fig. 8 for different choices of v_{sP}. Open circles represent ground truth measurements and are obtained from simulations using the direct method with pulsatile perturbations instead of step function inputs. For simulations of the adaptive phase-isostable reduced order equations, the update rule $\dot{p} = G_p(p, \theta, \psi_1) = -10^8(Q_1(\theta, p)\psi_1)$ is of the same form as (16). For simulations of the standard phase reduced Eq. (5), infinitesimal phase response curves associated with the periodic orbit for which $v_{sP} = 1.2$ nM are used. For different initial conditions that correspond to different phases on the $v_{sP} = 1.2$ nM periodic orbit, Fig. 9 compares the predicted and actual phase shifts that result when taking $v_{sP}(t) = 1.2 + 0.3(h(0) - h(L))$ nM. Here where L sets the duration of the pulse in v_{sP}. Panels A, B, and C show a single trial taking $L = 24$ hours with an initial condition of $\theta = 0$. Traces of $M_P(t)$ are shown in panel A. In response to the pulse, there is a slight mismatch in the timing of the outputs between the full model and the adaptive phase-isostable reduced order model; the phase-only reduction does not accurately reflect the response to the pulse. For the adaptive reduction, panel B shows the trace of $p(t)$ that results for the input shown in panel C. Panels D-G give representative results for initial conditions associated with different phases and for inputs of different duration. Here, $\Delta\theta \equiv \theta_a - \theta_e$ where θ_a is the phase resulting from the perturbation and θ_e is the phase that would have resulted had the perturbation not been applied. For short duration pulses, both the adaptive reduction and phase reduction strategies accurately predict the resulting phase shift. As the duration of the applied pulse is increased, the adaptive reduction strategy provides substantially more accurate results than the phase reduced equations.

5. Discussion and conclusion

Reduced order models based on the recently proposed adaptive phase-isostable reduction (13) are generally more accurate than models that use either standard phase reduction (2) or phase-isostable reduction (9) when large magnitude inputs are

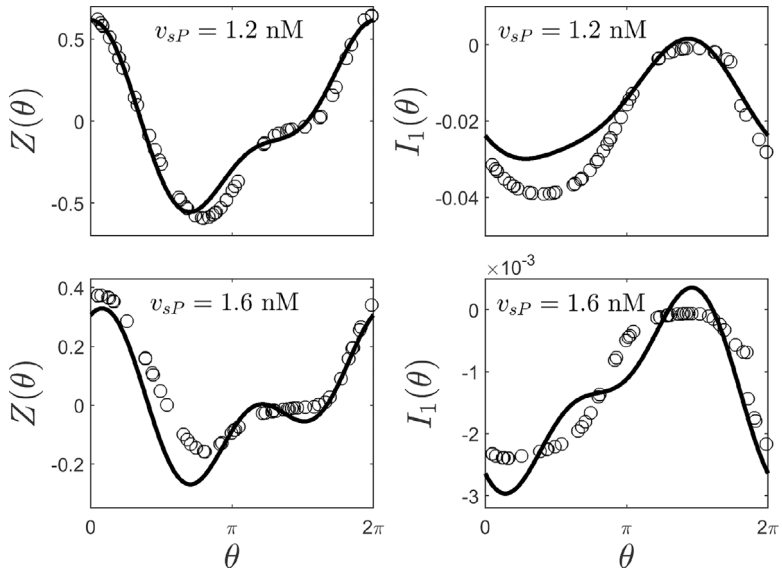

Fig. 8. Solid lines in each panel show infinitesimal phase and isostable response curves from (13) inferred using only information about $D(\theta, v_{sP})$ and $Q_1(\theta, v_{sP})$ from panels B and C of Fig. 7. Open circles represent ground truth datapoints obtained using Eq. (3) with pulse inputs.

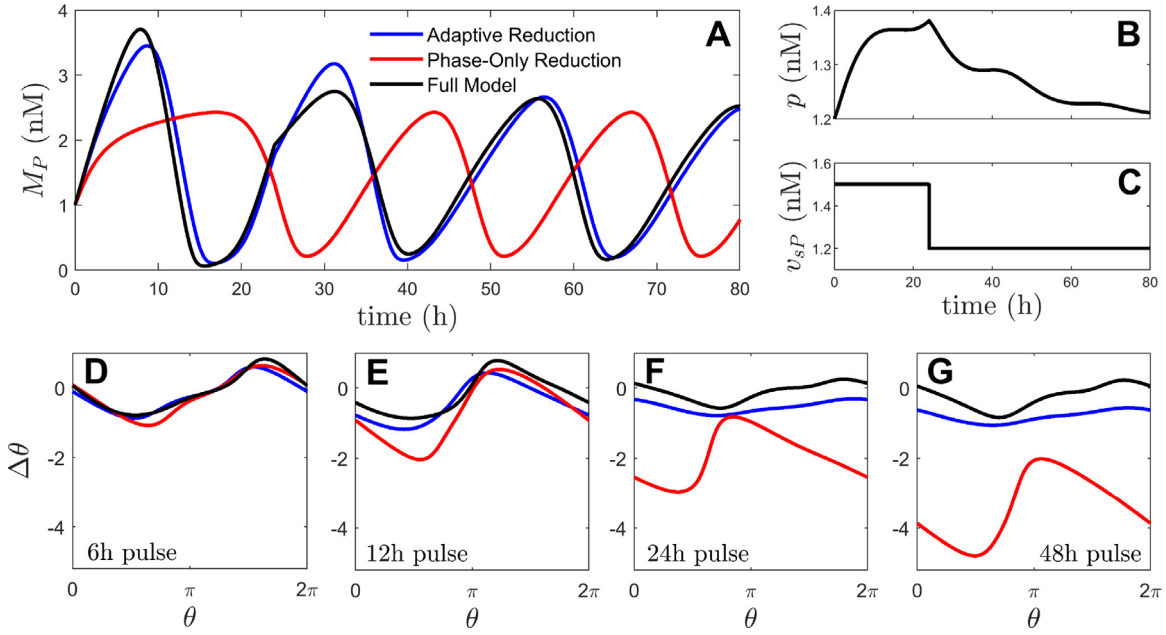

Fig. 9. For the circadian model, the input v_{sP} is elevated from 1.2 nM (corresponding to total darkness) to 1.5 nM (corresponding to a moderate light intensity) for a finite duration of time. Panel A shows the response to a 24 h duration pulse simulated using the adaptive reduction (13), phase-only reduction (5), and the full model equations (B.1)–(B.16). For the simulation from panel A, Panel B shows the time course of the variable p from the adaptive reduction and the associated input is shown in Panel C. Panels D-G aggregate results for different initial conditions (with different phases, θ) and for different pulse durations. On balance, both the adaptive reduction and phase reduction accurately predict the phase shift for short duration pulses in v_{sP}. For long duration pulses, the adaptive reduction approach substantially outperforms the standard phase reduction.

used. This work details a data-driven strategy to infer the necessary terms of the adaptive phase-isostable reduction from (13) which overcomes the limitations of these other reduction strategies highlighted in Fig. 1, i.e., that they do not accurately reflect system behavior when large magnitude inputs are applied.

The important implication from this work is that for a general system, provided it is possible to apply a series of either pulse inputs or step inputs and examine the relaxation to the underlying limit cycle, then it is also possible to obtain adaptive phase-isostable reduced order models of the form (13). As such, the proposed strategy requires no more information than the well-established direct method [2,9,10] and yields substantially more accurate reduced order models. By considering the change in the periodic orbit in response to static parameter perturbations in a basis of phase and isostable coordinates, the term of $D(\theta, p)$ can ultimately be written as an explicit function of the infinitesimal phase response curve $Z(\theta, p)$ using Eq. (34). Likewise, each $Q_j(\theta, p)$ can be written as an explicit function of the associated infinitesimal isostable response curve $I_j(\theta, p)$ using Eq. (35). In contrast to the approach suggested in [35], all the necessary terms of adaptive phase-isostable reduced equations can be obtained by either applying pulse inputs or step function inputs; using both types of inputs is not required and provides redundant information.

The proposed strategy is illustrated for three different models. In Section 4.1, a simple model with analytic solutions is considered to verify the derived relationships between the terms of the adaptive phase-isostable reduction. In Section 4.2, a series of pulse inputs is applied to infer the terms of the adaptive phase-isostable reduction in a conductance-based model neuron subject to noise in the transmembrane voltage variable. Section 4.3 considers only step function inputs to determine these terms for a computational model of the mammalian circadian clock. In each case, the adaptive reduction is substantially better at capturing the response to large magnitude inputs than the phase-only reduction.

The model identification strategy presented here relies on the adaptive phase-isostable reduction methodology. As such, it inherits the same limitations. For instance, it is only valid in regimes where the underlying model equations have oscillatory dynamics and cannot accommodate critical points of bifurcations in the allowable parameter sets. Additionally, the design of an appropriate parameter update rule G_p is not always straightforward when multiple isostable coordinates are considered. Also, the terms from the reduction from Eq. (13) must vary continuously with respect to both θ and p. As such, the underlying system equations must have a sufficient degree of smoothness. Additional limitations of the adaptive phase-isostable reduction strategy are discussed in [31].

As a matter of practical implementation, there is still much room for improvement in strategies for inference of the infinitesimal phase and isostable response curves. For instance, the model inference strategies described in Sections 4.2.1 and 4.3.1 do not give perfect approximations of the required response curves and Floquet exponents. These approximation issues are compounded in noisy environments where there must be a balance between using an input that is large enough discern a signal from the noisy data, but not so large as to drive the state too far away from the underlying limit cycle thereby invalidating the weak perturbation assumption. The development of more accurate strategies for data-driven inference of phase-isostable reduced order models of the form (9) would greatly benefit the adaptive phase-isostable model identification strategies presented here.

Declaration of competing interest

The authors declare that they have no known competing financial interests or personal relationships that could have appeared to influence the work reported in this paper.

Data availability

Data will be made available on request.

Acknowledgment

This material is based upon work supported by the National Science Foundation Grant No. CMMI-2140527.

Appendix A. Wang–Buzsaki model equations

Equations governing the Wang–Buzsaki model [40] considered in Section 4.2 are given below:

$$\begin{aligned} C\dot{V} &= -g_{\mathrm{Na}} m_\infty^3 h(V-E_{\mathrm{Na}}) - g_{\mathrm{K}} n^4 (V-E_K) - g_{\mathrm{L}}(V-E_{\mathrm{L}}) - i_w + i_{\mathrm{b}}, \\ \dot{h} &= \gamma\left[\alpha_h(V)(1-h) - \beta_h(V)h\right], \\ \dot{n} &= \gamma\left[\alpha_n(V)(1-n) - \beta_n(V)n\right], \\ \dot{w} &= a(1.5/(1+\exp((b-V)/k)) - w). \end{aligned} \tag{A.1}$$

Above, V represents the transmembrane voltage and h and n are gating variables. This model is augmented with an adaptation current [41], i_w, which is governed by the variable w. The baseline current, i_{b}, is chosen as the adaptive variable p. The membrane capacitance, $C = 1\ \mu\mathrm{F/cm}^2$. Auxiliary equations are

$$\begin{aligned} m_\infty(V) &= \alpha_m(V)/(\alpha_m(V)+\beta_m(V)), \\ \beta_n(V) &= 0.125\exp(-(V+44)/80), \\ \alpha_n(V) &= -0.01(V+34)/(\exp(-0.1(V+34))-1), \\ \beta_h(V) &= 1/(\exp(-0.1(V+28))+1), \\ \alpha_h(V) &= 0.07\exp(-(V+58)/20), \\ \beta_m(V) &= 4\exp(-(V+60)/18), \\ \alpha_m(V) &= -0.1(V+35)/(\exp(-0.1(V+35))-1). \end{aligned}$$

Reversal potentials and conductances are taken to be $E_{\mathrm{Na}} = 55$ mV, $E_{\mathrm{K}} = -90$ mV, $E_{\mathrm{L}} = -65$ mV, $g_{\mathrm{Na}} = 35\ \mathrm{mS/cm}^2$, $g_{\mathrm{K}} = 9\ \mathrm{mS/cm}^2$, $g_{\mathrm{L}} = 0.1\ \mathrm{mS/cm}^2$. $\gamma = 5$ influences the rate of change of the gating variables. The adaptation current is given by

$$i_w = g_w w(V - E_{\mathrm{K}}).$$

Parameters associated with the adaptation current are $a = 0.02\ \mathrm{m\ s}^{-1}$, $b = -5$ mV, $k = 0.5$ mV, $g_w = 2\ \mathrm{mS/cm}^2$.

Appendix B. Circadian model equations

The equations for the circadian model considered in Section 4.3 were presented in [42]. The model contains 16 variables. The mRNA concentrations of Per, Cry, and Bmal1 are denoted by M_P, M_C, and M_B, respectively. Phosphorylated (resp. nonphosphorylated) Per and Cry proteins in cytosol are denoted by P_{CP} and C_{CP} (resp., P_C and C_C). Concentrations of Per-Cry complex in cytosol and nucleus are denoted by PC_C, PC_N, PC_{CP}, and PC_{NP}; Concentrations of BMAL1 in cytosol and nucleus are denoted by B_C, B_{CP}, B_N, and B_{NP}. Here, the subscripts C, N, CP and NP denote cytosolic, nuclear, cytosolic phosphorylated, and phosphorylated forms, respectively. Finally, I_N denotes the inactive complex between Per-Cry and Clock-Bmal1 in the nucleus.

The model equations that govern the dynamics are:

$$\dot{M}_P = v_{sP}(t)\frac{B_N^n}{K_{AP}^n + B_N^n} - v_{mP}\frac{M_P}{K_{mP}+M_P} - k_{dmp}M_P, \tag{B.1}$$

$$\dot{M}_C = v_{sC}\frac{B_N^n}{K_{AC}^n + B_N^n} - v_{mC}\frac{M_C}{K_{mC}+M_C} - k_{dmc}M_C, \tag{B.2}$$

$$\dot{M}_B = v_{sB}\frac{K_{IB}^m}{K_{IB}^m + B_N^m} - v_{mB}\frac{M_B}{K_{mB}+M_B} - k_{dmb}M_B, \tag{B.3}$$

$$\begin{aligned} \dot{P}_C = {} & k_{sP}M_P - V_{1P}\frac{P_C}{K_p+P_C} + V_{2P}\frac{P_{CP}}{K_{dp}+P_{CP}} \\ & + k_4 PC_C - k_3 P_C C_C - k_{dn}P_C, \end{aligned} \tag{B.4}$$

$$\begin{aligned} \dot{C}_C = {} & k_{sC}M_C - V_{1C}\frac{C_C}{K_p+C_C} + V_{2C}\frac{C_{CP}}{K_{dp}+C_{CP}} \\ & + k_4 PC_C - k_3 P_C C_C - k_{dnc}C_C, \end{aligned} \tag{B.5}$$

$$\dot{P}_{CP} = V_{1P}\frac{P_C}{K_p+P_C} - V_{2P}\frac{P_{CP}}{K_{dp}+P_{CP}} - v_{dPC}\frac{P_{CP}}{K_d+P_{CP}} - k_{dn}P_{CP}, \tag{B.6}$$

$$\dot{C}_{CP} = V_{1C}\frac{C_C}{K_p+C_C} - V_{2C}\frac{C_{CP}}{K_{dp}+C_{CP}} - v_{dCC}\frac{C_{CP}}{K_d+C_{CP}} - k_{dn}C_{CP}, \tag{B.7}$$

$$\begin{aligned} \dot{PC}_C = {} & -V_{1PC}\frac{PC_C}{K_p+PC_C} + V_{2PC}\frac{PC_{CP}}{K_{dp}+PC_{CP}} - k_4 PC_C + k_3 P_C C_C \\ & + k_2 PC_N - k_1 PC_C - k_{dn}PC_C, \end{aligned} \tag{B.8}$$

$$\dot{PC}_N = -V_{3PC}\frac{PC_N}{K_p + PC_N} + V_{4PC}\frac{PC_{NP}}{K_{dp} + PC_{NP}} - k_2 PC_N + k_1 PC_C - k_7 B_N PC_N + k_8 I_N - k_{dn} PC_N, \tag{B.9}$$

$$\dot{PC}_{CP} = V_{1PC}\frac{PC_C}{K_p + PC_C} - V_{2PC}\frac{PC_{CP}}{K_{dp} + PC_{CP}} - v_{dPCC}\frac{PC_{CP}}{K_d + PC_{CP}} - k_{dn} PC_{CP}, \tag{B.10}$$

$$\dot{PC}_{NP} = -V_{3PC}\frac{PC_N}{K_p + PC_N} - V_{4PC}\frac{PC_{NP}}{K_{dp} + PC_{NP}} - v_{dPCN}\frac{PC_{NP}}{K_d + PC_{NP}} - k_{dn} PC_{NP}, \tag{B.11}$$

$$\dot{B}_C = k_{sB} M_B - V_{1B}\frac{B_C}{K_p + B_C} + V_{2B}\frac{B_{CP}}{K_{dp} + B_{CP}} - k_5 B_C + k_6 B_N - k_{dn} B_C, \tag{B.12}$$

$$\dot{B}_{CP} = V_{1B}\frac{B_C}{K_p + B_C} - V_{2B}\frac{B_{CP}}{K_{dp} + B_{CP}} - v_{dBC}\frac{B_{CP}}{K_d + B_{CP}} - k_{dn} B_{CP}, \tag{B.13}$$

$$\dot{B}_N = -V_{3B}\frac{B_N}{K_p + B_N} + V_{4B}\frac{B_{NP}}{K_{dp} + B_{NP}} + k_5 B_C - k_6 B_N - k_7 B_N PC_N + k_8 I_N - k_{dn} B_N, \tag{B.14}$$

$$\dot{B}_{NP} = V_{3B}\frac{B_N}{K_p + B_N} - V_{4B}\frac{B_{NP}}{K_{dp} + B_{NP}} - v_{dBN}\frac{B_{NP}}{K_d + B_{NP}} - k_{dn} B_{NP}, \tag{B.15}$$

$$\dot{I}_N = -k_8 I_N + k_7 B_N PC_N - v_{dIN}\frac{I_N}{K_d + I_N} - k_{dn} I_N. \tag{B.16}$$

Parameters are taken to be identical to basal values listed in Supplementary Table 1 of [42] with the exception of $k_1 = 0.58$ and $k_2 = 2.0$, which influence the kinetics of the nonphysphorylated cytosolic Per and Cry protein concentrations. The influence of light is incorporated by modulating v_{sP}, which sets the maximum rate of Per expression. In this work, $v_{sP} = 1.2$ nM/h corresponds to a state of total darkness and $v_{sP} = 1.8$ nM/h corresponds to a maximum level of brightness.

Appendix C. Adjoint method of solution for infinitesimal phase and isostable response curves

Consider a general equation of the form (1) with a periodic orbit x_p^γ with period $T(p)$. As discussed widely in the literature [4,43,44], $\frac{\partial\theta}{\partial x}$ associated with this periodic orbit can be computed by finding periodic solutions of the adjoint equation

$$\dot{a} = -J^T a, \tag{C.1}$$

where $a = \frac{\partial\theta}{\partial x}$ and J is the Jacobian, both evaluated at $x_p^\gamma(t)$. The periodic solution of Eq. (C.1) must be appropriately normalized so that $\frac{2\pi}{T(p)} = F(x_p^\gamma, p)\cdot a(x_p^\gamma)$, where the dot denotes the dot product. Similarly, as discussed in [20], the gradient of the jth isostable coordinate can be found as the periodic solution of

$$\dot{b}_j = -(J^T - \kappa_j \mathrm{Id})b_j, \tag{C.2}$$

where $b_j = \frac{\partial\psi_j}{\partial x}$ evaluated at $x_p^\gamma(t)$, κ_j is the Floquet exponent associated with ψ_j, and Id is an appropriately sized identity matrix. For stable periodic orbits, periodic solutions of Eq. (C.1) can be solved by integrating backwards in time until transients decay. Periodic solutions of (C.2) are generally unstable but can be obtained using a Newton iteration or using a bi-orthogonalization method proposed in [45].

Appendix D. Identification of reduced order model parameters using operational phase coordinates

As discussed in Section 2.4, operational phase coordinates can be used to obtain information about transient behavior associated with the decay of solutions to an underlying stable limit cycle. In this work, results from [23] are leveraged to accomplish this task, with useful results summarized in Eqs. (17)–(19). This appendix is provided to clearly illustrate how Eqs. (17)–(19) from the main text can be obtained using results that were previously presented in [23].

In this work, θ and θ^* represent asymptotic and operational phase coordinates, respectively, for a stable limit cycle x_p^γ that emerges in Eq. (1) when $u = p$ is held constant. As illustrated in Eq. (15) from Ref. [23], if u is held at p, when considering a single isostable coordinate ψ_1 in the reduced order model, to leading order ϵ the time between the kth crossing of the $\theta = 0$ and $\theta^* = 0$ level set is related by

$$t_k^* = t_k - \frac{\psi_1(t_k)(n \cdot g_1(0,p))}{n \cdot \dot{x}_p^\gamma|_{\theta=0}}. \tag{D.1}$$

where t_k^* corresponds to the kth crossing of the $\theta^* = 0$ level set, t_k corresponds to the kth crossing of the $\theta^* = 0$ level set, $g_1(0,p)$ is the Floquet eigenfunction associated with the ψ_1 isostable coordinate evaluated at $\theta = 0$, $\dot{x}_p^\gamma|_{\theta=0}$ is the time derivative of the periodic orbit evaluated at $\theta = 0$, n is a unit vector normal to the $\theta^* = 0$ level set, and the dot denotes the dot product. Additionally, Ref. [23] defines the following constant

$$\alpha_1 = \frac{\omega(p)\kappa_1(p)(n \cdot g_1(0,p))}{n \cdot \dot{x}_p^\gamma|_{\theta=0}}. \tag{D.2}$$

Note that $g_1(\theta, p)$ is a Floquet eigenfunction which is unique to a constant scaling; in this work, it is assumed that $n \cdot \dot{x}_p^\gamma|_{\theta=0} \neq 0$ so that the normalization $\alpha_1 = 1$ can be mandated with an appropriate scaling of $g_1(\theta, p)$. Combining Eqs. (D.1) and (D.2) yields Eq. (17) from the main text. Eq. (18) from the main text can be obtained through algebraic manipulation of Eq. (D.2) recalling the scaling $\alpha_1 = 1$ and noting that $\frac{dx^\gamma}{dt} = \omega\frac{dx^\gamma}{d\theta}$. Eq. (19) from the main text can be derived starting with Equation (39) from [23]:

$$\log(\tau_n) = \alpha + n\log(\lambda_1), \tag{D.3}$$

where $\tau_n = t_{n+1}^* - t_n^* - T(p)$, where t_n^* is the nth crossing of the $\theta^* = 0$ level set when u is held constant at p, α is a constant that depends on system parameters and initial conditions, $T(p) = 2\pi/\omega(p)$ is the period of the limit cycle, and λ_1 is the Floquet multiplier associated with the isostable coordinate ψ_1. Considering Eq. (D.3) at successive indices n and $n+1$, through direct manipulation one finds

$$\log(\lambda_1) = \log(\tau_{n+1}/\tau_n). \tag{D.4}$$

Eq. (19) follows directly from the relation $\kappa_1(p) = \log(\lambda_1)/T(p)$ which is a standard relationship between Floquet exponents and Floquet multipliers.

References

[1] Y. Kuramoto, Chemical Oscillations, Waves, and Turbulence, Springer-Verlag, Berlin, 1984.
[2] A. Winfree, The Geometry of Biological Time, second ed., Springer Verlag, New York, 2001.
[3] E.M. Izhikevich, Dynamical Systems in Neuroscience: The Geometry of Excitability and Bursting, MIT Press, London, 2007.
[4] G.B. Ermentrout, D.H. Terman, Mathematical Foundations of Neuroscience, Vol. 35, Springer, New York, 2010.
[5] E. Brown, P. Holmes, J. Moehlis, Globally coupled oscillator networks, in: Perspectives and Problems in Nonlinear Science, Springer, 2003, pp. 183–215.

[6] D. Wilson, J. Moehlis, Optimal chaotic desynchronization for neural populations, SIAM J. Appl. Dyn. Syst. 13 (1) (2014) 276–305.
[7] M.A. Schwemmer, T.J. Lewis, The theory of weakly coupled oscillators, in: Phase Response Curves in Neuroscience, Springer, 2012, pp. 3–31.
[8] B. Pietras, A. Daffertshofer, Network dynamics of coupled oscillators and phase reduction techniques, Phys. Rep. (2019).
[9] L. Glass, M.C. Mackey, From Clocks to Chaos: The Rhythms of Life, Princeton University Press, Princeton, 1988.
[10] T. Netoff, M.A. Schwemmer, T.J. Lewis, Experimentally estimating phase response curves of neurons: theoretical and practical issues, in: Phase Response Curves in Neuroscience, Springer, 2012, pp. 95–129.
[11] J. Cui, C.C. Canavier, R.J. Butera, Functional phase response curves: A method for understanding synchronization of adapting neurons, J. Neurophysiol. 102 (1) (2009) 387–398.
[12] T.I. Netoff, C.D. Acker, J.C. Bettencourt, J.A. White, Beyond two-cell networks: experimental measurement of neuronal responses to multiple synaptic inputs, J. Comput. Neurosci. 18 (3) (2005) 287–295.
[13] J. Foss, J. Milton, Multistability in recurrent neural loops arising from delay, J. Neurophysiol. 84 (2) (2000) 975–985.
[14] W. Kurebayashi, S. Shirasaka, H. Nakao, Phase reduction method for strongly perturbed limit cycle oscillators, Phys. Rev. Lett. 111 (21) (2013) 214101.
[15] Y. Park, B. Ermentrout, Weakly coupled oscillators in a slowly varying world, J. Comput. Neurosci. 40 (3) (2016) 269–281.
[16] K. Pyragas, V. Novičenko, Phase reduction of a limit cycle oscillator perturbed by a strong amplitude-modulated high-frequency force, Phys. Rev. E 92 (1) (2015) 012910.
[17] C.O. Diekman, A. Bose, Entrainment maps: a new tool for understanding properties of circadian oscillator models, J. Biol. Rhythms 31 (6) (2016) 598–616.
[18] C.O. Diekman, A. Bose, Reentrainment of the circadian pacemaker during jet lag: east–west asymmetry and the effects of north-south travel, J. Theoret. Biol. 437 (2018) 261–285.
[19] D. Jordan, P. Smith, Nonlinear Ordinary Differential Equations: An Introduction for Scientists and Engineers, Vol. 10, Oxford University Press, Oxford, 2007.
[20] D. Wilson, J. Moehlis, Isostable reduction of periodic orbits, Phys. Rev. E 94 (5) (2016) 052213.
[21] K.C.A. Wedgwood, K.K. Lin, R. Thul, S. Coombes, Phase–amplitude descriptions of neural oscillator models, J. Math. Neurosci. 3 (1) (2013) 2.
[22] B. Letson, J.E. Rubin, LOR for analysis of periodic dynamics: A one-stop shop approach, SIAM J. Appl. Dyn. Syst. 19 (1) (2020) 58–84.
[23] D. Wilson, B. Ermentrout, An operational definition of phase characterizes the transient response of perturbed limit cycle oscillators, SIAM J. Appl. Dyn. Syst. 17 (4) (2018) 2516–2543.
[24] O. Castejón, A. Guillamon, G. Huguet, Phase–amplitude response functions for transient-state stimuli, J. Math. Neurosci. 3 (2013) 13.
[25] M. Rosenblum, A. Pikovsky, Numerical phase reduction beyond the first order approximation, Chaos 29 (1) (2019) 011105.
[26] A. Guillamon, G. Huguet, A computational and geometric approach to phase resetting curves and surfaces, SIAM J. Appl. Dyn. Syst. 8 (3) (2009) 1005–1042.
[27] D. Wilson, Phase–amplitude reduction far beyond the weakly perturbed paradigm, Phys. Rev. E 101 (2) (2020) 022220.
[28] D. Wilson, B. Ermentrout, Greater accuracy and broadened applicability of phase reduction using isostable coordinates, J. Math. Biol. 76 (1–2) (2018) 37–66.
[29] D. Wilson, B. Ermentrout, Phase models beyond weak coupling, Phys. Rev. Lett. 123 (16) (2019) 164101.
[30] Y. Park, D. Wilson, High-order accuracy computation of coupling functions for strongly coupled oscillators, SIAM J. Appl. Dyn. Syst. 20 (3) (2021) 1464–1484.
[31] D. Wilson, An adaptive phase–amplitude reduction framework without $\mathcal{O}(\epsilon)$ constraints on inputs, SIAM J. Appl. Dyn. Syst. 21 (1) (2022) 204–230.
[32] A. Mauroy, I. Mezić, J. Moehlis, Isostables, isochrons, and koopman spectrum for the action–angle representation of stable fixed point dynamics, Physica D 261 (2013) 19–30.
[33] I. Mezić, Spectrum of the Koopman operator, spectral expansions in functional spaces, and state-space geometry, J. Nonlinear Sci. (2019) 1–55.
[34] D. Wilson, A data-driven phase and isostable reduced modeling framework for oscillatory dynamical systems, Chaos 30 (1) (2020) 013121.
[35] D. Wilson, Optimal control of oscillation timing and entrainment using large magnitude inputs: An adaptive phase–amplitude-coordinate-based approach, SIAM J. Appl. Dyn. Syst. 20 (4) (2021) 1814–1843.
[36] J. Guckenheimer, Isochrons and phaseless sets, J. Math. Biol. 1 (3) (1975) 259–273.
[37] I. Mezić, Spectrum of the koopman operator, spectral expansions in functional spaces, and state-space geometry, J. Nonlinear Sci. 30 (5) (2020) 2091–2145.
[38] M.D. Kvalheim, S. Revzen, Existence and uniqueness of global koopman eigenfunctions for stable fixed points and periodic orbits, Physica D (2021) 132959.
[39] Y. Wang, J.P. Gill, H.J. Chiel, P.J. Thomas, Shape versus timing: linear responses of a limit cycle with hard boundaries under instantaneous and static perturbation, SIAM J. Appl. Dyn. Syst. 20 (2) (2021) 701–744.
[40] X.J. Wang, G. Buzsáki, Gamma oscillation by synaptic inhibition in a hippocampal interneuronal network model, J. Neurosci. 16 (20) (1996) 6402–6413.
[41] B. Ermentrout, Linearization of FI curves by adaptation, Neural Comput. 10 (7) (1998) 1721–1729.
[42] J.C. Leloup, A. Goldbeter, Toward a detailed computational model for the mammalian circadian clock, Proc. Natl. Acad. Sci. 100 (12) (2003) 7051–7056.
[43] E. Brown, J. Moehlis, P. Holmes, On the phase reduction and response dynamics of neural oscillator populations, Neural Comput. 16 (4) (2004) 673–715.
[44] F.C. Hoppensteadt, E.M. Izhikevich, Weakly Connected Neural Networks, Springer, New York, 1997.
[45] S. Shirasaka, W. Kurebayashi, H. Nakao, Phase–amplitude reduction of transient dynamics far from attractors for limit-cycling systems, Chaos 27 (2) (2017) 023119.